

The Catalan magnetic anomaly: Its significance for the crustal structure of the Gulf of Lion passive margin and relationship to the Catalan transfer zone

Albane Canva, Isabelle Thinon, Aurélie Peyrefitte, Renaud Couëffé, Agnès Maillard, Laurent Jolivet, Guillaume Martelet, Frédéric Lacquement, Pol Guennoc

▶ **To cite this version:**

Albane Canva, Isabelle Thinon, Aurélie Peyrefitte, Renaud Couëffé, Agnès Maillard, et al.. The Catalan magnetic anomaly: Its significance for the crustal structure of the Gulf of Lion passive margin and relationship to the Catalan transfer zone. Marine and Petroleum Geology, 2020, 113, pp.104174. 10.1016/j.marpetgeo.2019.104174 . hal-03488689

HAL Id: hal-03488689
https://hal.science/hal-03488689

Submitted on 21 Jul 2022

HAL is a multi-disciplinary open access archive for the deposit and dissemination of scientific research documents, whether they are published or not. The documents may come from teaching and research institutions in France or abroad, or from public or private research centers.

L'archive ouverte pluridisciplinaire **HAL**, est destinée au dépôt et à la diffusion de documents scientifiques de niveau recherche, publiés ou non, émanant des établissements d'enseignement et de recherche français ou étrangers, des laboratoires publics ou privés.



Distributed under a Creative Commons Attribution - NonCommercial 4.0 International License

Version of Record: https://www.sciencedirect.com/science/article/pii/S0264817219306282
Manuscript_aac53bed13e3c962e47de3dc46aa4843

The Catalan magnetic anomaly: Its significance for the crustal structure of the Gulf of Lion passive margin and relationship to the Catalan transfer zone

Albane Canva[a*], Isabelle Thinon[a*], Aurélie Peyrefitte[a*], Renaud Couëffé[a], Agnès Maillard[b], Laurent Jolivet[c], Guillaume Martelet[a], Frédéric Lacquement[a], Pol Guennoc[a]

[a]BRGM, GeoResources Division, 3 avenue Claude Guillemin, 45 060 Orleans, France

[b]GET, UMR 5563, Observatoire Midi-Pyrénées, 14 avenue Edouard Belin, 31400 Toulouse, France

[c]ISTEP, Sorbonne Université, Rue de l'école de Médécine, 75 006 Paris, France

[*] Corresponding author.

Fax: + 33 2 38 64 33 33.

E-mail address: albanecanva@msn.com (A. Canva); a.peyrefitte@brgm.fr (A. Peyrefitte); i.thinon@brgm.fr (I. Thinon).

BRGM, DGR/GBS, 3 avenue Claude Guillemin, 45 100 Orléans, France

© 2019 published by Elsevier. This manuscript is made available under the CC BY NC user license
https://creativecommons.org/licenses/by-nc/4.0/

ABSTRACT

The western part of the Gulf of Lion (GoL) passive margin, at the foot of the Pyrenees mountain chain hosts the Catalan magnetic anomaly (CMA), a significant NW-SE-trending linear magnetic anomaly 50 km long with no associated gravimetric signal. The CMA is located on the continental slope near the NW-SE-trending Catalan transfer zone (CTZ), and it extends from the shelfbreak to the abyssal plain across thinned to hyper-thinned continental domain. This study interprets an updated geophysical dataset to better understand the Pyrenees–GoL transition and proposes a new interpretation of the CMA's source. Gravimetric and magnetic modelling of the lithosphere along two perpendicular cross-sections indicates that the CMA is generated by a magnetic body (80 × 20 × 12 km) , called here the Catalan body within the thinned continental domain. We interpret it as a mass of mafic material underplating and intruding the continental crust along a crustal fault belonging to the CTZ system. From the new map of Moho depths, a wide NW-SE-trending zone is highlighted on the western extremity of the GoL margin at the foot of the eastern Pyrenees Chain. It is characterized by (i) a heterogeneous crustal structure and mantle rise underneath the Tertiary Catalan sedimentary basin in the continental shelf area, (ii) a necking zone in a more proximal location compared to the eastern GoL margin, and (iii) the presence of the magmatism (Catalan body) under and in the thinned continental crust, in the necking zone domain. These characteristics may be induced by the transtensional motion along the CTZ during the Tertiary opening of the Liguro-Provençal Basin, contemporary with the extension of the GoL margin. However, the role of inherited structures from the Hercynian orogeny, Mesozoic rifting and Pyrenean orogeny cannot be excluded when explaining the crustal heterogeneity, transfer zones and Moho morphology in this region.

Keywords:

Gulf of Lion margin, Pyrenees, Catalan magnetic anomaly, Magnetic and gravimetric modelling, Moho depth map, Transfer zone, Mafic magmatic intrusion, Underplating

1. Introduction

The formation of mountain ranges and subsequent postorogenic thinning are major topics of debate. In the western Mediterranean, the Pyrenean orogenic belt ends abruptly at the Gulf of Lion (GoL) passive margin, and after decades of work in this area, explaining this termination of the eastern Pyrenees remains a challenge.

Between the Pyrenees and the GoL margin (**Fig. 1**), a major transfer zone called the Catalan transfer zone (CTZ; Mauffret *et al.*, 2001) is widely considered to have played a major role in the opening of the GoL and the Liguro-Provençal Basin. The position of the CTZ also coincides with the edge of a major magnetic anomaly (**Fig. 1**). Since 1965, when comprehensive aeromagnetic data were first acquired in this region, published hypotheses have not resulted in realistic interpretations of this anomaly, which is a key feature of the GoL margin.

Magnetic anomalies are relatively common features of rift systems, such as the East Africa rift (e.g. Buck, 2006), the Aden-Afar rift (e.g. Bridges *et al.*, 2012) and the Red Sea rift (e.g. Ligi *et al.*, 2018). They also are common on volcanic continental margins, such as the Vøring and Namibia margins (e.g. White *et al.*, 1987; Geoffroy, 2005; Bauer *et al.*, 2000), and are known in nonvolcanic margins as well. These magnetic anomalies have been interpreted variously as indicating the presence of mafic intrusions in the exhumed or hyperextended continental crust (Northern Red Sea margin, Ligi *et al.*, 2018; Galicia passive margin, Schärer *et al.*, 1995; Iberian margin, Neres *et al.*, 2018), mafic underplating coupled with basaltic intrusions (Newfoundland-Iberia rift system, Bronner *et al.*, 2011; Thybo & Artemieva, 2013), or strongly serpentinized mantle (e.g. Dunlop & Prévot, 1982; Shive *et al.*, 1988; Sibuet *et al.*, 2007). In the Liguro-Provençal Basin and Valencia Trough, volcanic edifices have been shown to be related to subduction slab retreat (e.g. Maillard & Mauffret, 1999; Séranne, 1999; Jolivet & Faccenna, 2000; Jolivet *et al.*, 2006; Réhault *et al.*, 2012; **Fig. 1** and **Fig. 2**). Some of those volcanic bodies also coincide with strong magnetic anomalies (Maillard & Mauffret, 1993; Rollet *et al.*, 2002).

The significant NW-SE-trending magnetic anomaly in the southwestern GoL (**Fig. 1**) is called hereafter the Catalan magnetic anomaly (CMA), due to its location off the coast of the Catalan region.

A smaller but almost as intense magnetic anomaly to the east of the CMA is called anomaly B hereafter

In this paper, we interpret both magnetic anomalies, with a special focus on the CMA, using magnetic and gravimetric modelling along two cross-sections (M1 and M2 in **Fig. 2**). We propose a consistent geological interpretation of these anomalies in terms of crustal geometry and an explanation of the role of the structures associated with them in the transition between the Pyrenees and the GoL.

2. Geological setting

The GoL margin (**Fig. 2**) is a segment of the northern continental margin of the Liguro-Provençal oceanic basin, which is interpreted as a back-arc basin that formed as a result of the 30° anticlockwise rotation of the Corsica-Sardinia block during the retreating phase of Apennine subduction (e.g. Réhault *et al.*, 1984; Gueguen *et al.*, 1998; Jolivet & Faccenna, 2000; Gattacceca *et al.*, 2007; Jolivet *et al.*, 2015). The Liguro-Provençal Basin opened in two steps: a synrift stage (Chattian to early Burdigalian, 30–20.5 Ma) and a postrift stage (early Burdigalian to Langhian, 20.5–15 Ma) (e.g. Gattacceca *et al.*, 2007).

From the rifting phase into Quaternary time, volcanism has been active in the Catalan region (e.g. Bartrina *et al.*, 1992; Mauffret *et al.*, 2001), the Valencia Trough (Marti *et al.*, 1992; Maillard, 1993; Maillard & Mauffret, 1993) and the West Mediterranean basin. In Languedoc, long-lasting - Mesoszoic to Quaternary- alkakine volcanic activity trending N-S over 160 km is related to a lithospheric mantle anomaly (Liotard *et al.*, 1991; Dautria *et al.*, 2010). In the Corsica Liguria basins, the oldest Tertiary magmatism related to the Western Mediterranean geodynamics, was mainly calc-alkaline and dated at ca 35 Ma (e.g. Réhault *et al.*, 2012). Volcanic activity in the Miocene and Pliocene was important on the Provence, Sardinia and Corsica margins (e.g. Réhault *et al.*, 2012). These volcanic events may be an expression of hot mantle upwelling linked to the development of a slab window in a postcollisional tectonic framework (Réhault *et al.*, 2012; Jolivet & Faccenna, 2000).

During the anticlockwise rotation of the Corsica-Sardinia block, major transfer zones such as the Catalan and Arlesian transfer zones appear to have played a key role in segmenting the Liguro-Provençal domain into the Valencia Trough, the GoL margin and the Provençal margin (**Fig. 1** and **2**;

e.g. Gorini, 1993; Guennoc *et al.*, 1994, 2000; Mauffret *et al.*, 1995, 2001; Benedicto et al, 1996; Mauffret & Gorini, 1996; Olivet, 1996; Gueguen *et al.*, 1998; Gattacceca *et al.*, 2007; Séranne *et al.*, 1995; Maillard & Mauffret, 1999). These transfer zones were inferred by researchers for kinematic reasons, but they are difficult to detect in observations, and no systematic study has been undertaken to characterize their nature or their geometries.

2.1. The Gulf of Lion margin

The GoL continental margin extends southeast of the Cévennes fault between the Provence region to the east and the Pyrenees chain and Roussillon basin to the west (**Fig. 1** and **Fig. *2***). The margin is conventionally divided into five crustal domains, from the present coast to the oceanic crust, on the basis of the ECORS and SARDINIA deep seismic reflection profiles (**Fig. 3**; Gorini, 1993; Séranne, 1999; Gailler *et al.*, 2009; Bache *et al.*, 2010; Moulin *et al.*, 2015). The unthinned continental crust domain (30 km thick) is composed of a lower and upper crust, both about 15–17 km thick. The Hinge zone is the domain where the crust thins seaward from ~30 to 20 km. Further offshore, domain I (**Fig. 1**, **Fig. *2*** and **Fig. *3***) is about 170 km wide and consists of thinned to hyper-thinned continental crust (20 km to 5 km thick) featuring horsts, grabens and tilted blocks in the upper continental crust and a thinned lower continental crust (Gorini, 1993; Séranne *et al.*, 1995; Gailler *et al.*, 2009; Moulin *et al.*, 2015). Its seaward edge is a slope area in which the crust thins from 20 to 7 km. On the SARDINIA profile, the slope area is associated with a high-velocity body (6.5–7 km/s, **Fig. 3**B; Moulin *et al.*, 2015). All along the GoL margin, domain II, a transitional domain around 100 km wide, is characterized by a crust 5 km thick with anomalously high velocities (7–7.5 km/s, **Fig. 3**; Seranne, 1999; Moulin *et al.*, 2015). This very thin crust is interpreted as either exhumed and partially serpentinized upper mantle (Boillot *et al.*, 1980, 1987, 1989; Beslier *et al.*, 1993; Guennoc *et al.*, 1994; Chamot-Rooke *et al.*, 1999; Gailler *et al.*, 2009) or exhumed and thinned/stretched lower continental crust (Wernicke, 1985; Séranne *et al.*, 1995; Séranne, 1999; Moulin *et al.*, 2005, 2015; Aslanian *et al.*, 2009; Jolivet *et al.*, 2015). Domain III consists of thin (5 km) oceanic crust (e.g. Pascal *et al.*, 1993; Chamot-Rooke *et al.*, 1999; Rollet *et al.*, 2002; Gailler *et al.*, 2009).

In domain I on the continental shelf of the GoL margin, extensional structures predominantly oriented NE-SW and their onshore counterparts overprint the Pyrenean fold-and-thrust belt. The interaction of this extension tectonic features with inherited Pyrenean structures has been analysed by some authors (Mauffret *et al.* 1995, 1996, 2001; Séranne *et al.*, 1995; Benedicto *et al.*, 1996). The GoL shelf is divided into two distinct parts (**Fig. 2**). The northeastern part is characterized by a succession of horsts and grabens oriented NE-SW with a thin (<2 km) cover of Cenozoic synrift and postrift sedimentary formations (Guennoc *et al.*, 2000; Oudet *et al.*, 2010). The southwestern part contains the wide and deep Graben Central basin, which encompasses the Catalan and Cathares basins (**Fig. 2**). Both of these basins are filled by 6 km of Cenozoic synrift and postrift sediments (Gorini, 1993; Gorini *et al.*, 1994; Guennoc *et al.*, 2000; Bache *et al.*, 2010) and are separated by a transfer zone (n°1 on **Fig. 2**) associated with a step in Moho depth from 21 to 24 km (Mauffret *et al.*, 2001). The Catalan basin is underlain by a moderately thin crust and a shallow Moho (21 km from seismic data in Mauffret *et al.*, 2001, **Fig. 3**C; 15 km from gravity modelling in Guennoc *et al.*, 1994). The Moho is deeper (23–28 km) along the Catalan margin and below the so-called Rascasse horst (**Fig. 3**C). The Rascasse horst is a structure interpreted as a rollover on a deep crustal detachment (Mauffret *et al.*, 2001). Several interpretations have been proposed to explain the establishment of these sedimentary basins. The Catalan basin may be a Mesozoic basin, formed during Jurassic extension or Cretaceous pull-apart motion, into which the Rascasse structure then slid during the Pyrenean orogeny and was afterward displaced to its present position along a deep detachment during extension (Mauffret *et al.*, 2001). The Graben Central basin could be related to the Liguro-Provençal back-arc rifting (e.g. Réhault *et al.*, 1984; Mauffret *et al.*, 1995) or the southward Tertiary extension of the West European Continental Rift system (Gorini, 1993; Séranne, 1999; **Fig. 2**), which ran from the Rhine graben to the Valencia basin during an episode of E-W extension (Bergerat, 1987; Ziegler, 1992). According to Séranne (1999), these rift basins are controlled by NE-trending extensional faults overprinting the E-W-trending Pyrenean thrusts in the Provence and Languedoc regions.

The prerift substratum of the GoL margin is composed of Paleozoic and Mesozoic formations (**Fig. 2**). The Palaeozoic substratum includes various lithologies (such as metasediments pelites, schists, sandstones, limestones or granite) from the Variscan cycle (Guennoc *et al.*, 2000) and is

deformed by NE-SW-trending faults (Nîmes, Cévennes, Alès, and others) related to the late-Variscan strike-slip and Tethyan rifting (e.g. Arthaud & Matte, 1975; Mascle *et al.*, 1996). Offshore, deep detachments have been described in the basement beneath the Tramontane well (Gorini *et al.*, 1994) and the Rascasse well (Guennoc *et al.*, 1994; **Fig. 3**C). In the western GoL, seismic profiles and well samples show the Mesozoic sedimentary cover (sampled in Calmar or Agde Maritime 1 wells; Guennoc *et al.*, 2000) to be thin (as seen on seismic profiles), unlike the thick Mesozoic cover in the Pyrenean sedimentary basins (Boucheville, Bas Agly and St. Paul de Fenouillet synclines to the north of the North Pyrenean Fault and the Figueres-Montgrí basin to the south, **Fig. 2**; e.g. Vergés *et al.*, 2002; Lagabrielle *et al.*, 2010; Tugend *et al.*, 2014; Clerc *et al.*, 2015; Chelalou *et al.*, 2016; Teixell *et al.*, 2016; Wang *et al.*, 2016; Tavani *et al.*, 2018) and in the eastern GoL margin (as presumed from seismic profiles; Mauffert & Gorini, 1996) and Provençal margin (Beausset syncline, **Fig. 2**; Bestani *et al.*, 2015; Fournier *et al.*, 2016).

2.2. The eastern Pyrenees

The interactions between the Pyrenean thrusts and the GoL rifting are not fully understood. The extent to which lithospheric heterogeneities inherited from the Hercynian and Pyrenean orogenies and Mesozoic (Permian or mid-Cretaceous) rifting influenced the geometry and kinematics of the GoL margin is an open question.

The Pyrenean belt (**Fig. 2** inset) is the result of the convergence between the Iberian and European plates starting in the Late Cretaceous (e.g. Choukroune et al., 1973; Olivet, 1996). Metamorphosed Mesozoic sedimentary formations are distributed in a narrow WNW-ESE-trending belt defined as the North Pyrenean Zone, bounded by two major post-metamorphic thrusts, the North Pyrenean Fault (NPF) to the south and the North Pyrenean Frontal Thrust to the north. Outcrops of subcontinental peridotite in the North Pyrenean Zone are attributed to mantle exhumation and crustal hyperextension during the Mesoszoic rift-transtensional motions (Vielzeuf & Kornprobst, 1984; Lagabrielle & Bodinier, 2008; Clerc *et al.*, 2015; Teixell *et al.*, 2016). At a regional scale, the North Pyrenean Zone is thought to represent the portion of the lithosphere that accommodated most of the deformation during the anticlockwise rotation of the Iberian plate with respect to the European plate in mid-Cretaceous times (Choukroune & Mattauer, 1978).

A recent study by Wehr *et al.* (2018), citing passive seismic profiles across the Pyrenees (Diaz *et al.*, 2018; Chevrot *et al.*, 2018), presented a 3D geometrical model of Bouguer anomalies showing a Moho deeper than 50 km below the Pyrenean axial zone that is shallower (30–40 km) in the eastern part (the Cap de Creus region). Wehr *et al.* (2018) concluded that the shallower Moho signifies a missing lower crust, a possible consequence of the retreat of the Tyrrhenian slab during the opening of the western Mediterranean basins. The Bouguer model also displays a shallowing of the Moho from 30 to 25 km in an E-W-trending area under the Roussillon basin. Wehr *et al.* (2018) proposed that the North Pyrenean Fault extends below the Roussillon basin and accounts for this step in the Moho depth. Other authors have proposed extensions of the North Pyrenean Fault into the western GoL, lying north of the Catalan basin from seismic data (Mauffret *et al.*, 2001) and north of the Rascasse horst from aeromagnetic data (Guennoc *et al.*, 1994). The fault is not inferred in the eastern GoL. Some authors draw it at the foot of the GoL and Provençal continental margin (e.g. Guennoc *et al.*, 1994; Séranne, 1999).

In the Cap de Creus region, the Variscan basement contains intrusions of diorite and other granitoids (e.g. Carreras, 2001; Carreras *et al.*, 2004; Druguet, 2001) and NW-SE-trending shear zones. Tertiary reactivation of these shear zones has been proposed at 58.57 ± 0.55 Ma (Vissers *et al.*, 2016) or at 69–47 Ma and 42–37 Ma (Monié *et al.*, 2018; Druguet *et al.*, 2018), synchronously with Pyrenean compression. The thrust sheet involving the Figueres-Montgrí basin has been dismembered by a series of Neogene NW-SE-trending extensional faults associated with the North Balearic fault zone (NBFZ) (Mauffret *et al.*, 2001).

2.3. The Catalan transfer zone

Most kinematic reconstructions imply that the rotation of the Corsica-Sardinia block involved motion along a series of NW-SE transfer zones (e.g. NBFZ, CTZ, Arlesienne transfer zone; **Fig. 1**), but these systems have never been clearly imaged and their structures are elusive (Auzende *et al.*, 1973; Réhault *et al.*, 1984; Maillard *et al.*, 2003; Granado *et al.*, 2016). In particular, the abrupt transition between the GoL margin and the eastern Pyrenees appears to coincide with the poorly constrained CTZ (Lefebvre, 1981; Gorini *et al.*, 1993; Séranne *et al.*, 1995; Mauffret *et al.*, 2001). The CTZ runs along the Catalan margin in the Cap de Creus region (**Fig. 2**), where there is an abrupt

thickening of the crust and a dipping of the Moho toward the Pyrenees (e.g. Nercessian *et al.*, 2001; Wehr *et al.*, 2018), and below the Rascasse horst (Mauffret *et al.*, 2001). The CTZ plays a major role on tectonics and sedimentation in this area and has accommodated transtensional / extensional deformation of the Rascasse horst and the coeval opening of the Catalan basin (Mauffret *et al.*, 1995, 2001).

Further south and slightly to the west, the NBTZ (e.g. Auzende *et al.*, 1973; Rehault *et al.*, 1984; Séranne, 1999) (Fig. 1) separates the Valencia Trough from the deep Liguro-Provençal Basin and marks the trace of the Corsica-Sardinia block during its Miocene rotation (**Fig. 2** inset; Séranne, 1999; Maillard & Mauffret, 1999; Mauffret *et al.*, 2001).

2.4. The Catalan magnetic anomaly

The CMA appears on the magnetic map of the western Mediterranean Sea (Galdeano & Rossignol, 1977) as a strong linear magnetic anomaly (**Fig. 1**). Seismic reflection profiles (Gorini *et al.*, 1993; Guennoc *et al.*, 1994; Mauffret *et al.*, 2001) show no evidence of volcanic intrusions in the postrift and synrift sedimentary cover in the CMA area (Catalan basin and Rascasse horst; **Fig. 2**).

From gravity modelling, Guennoc *et al.* (1994) interpreted a possible mantle rise under the Catalan basin that is in accordance with Mauffret *et al.* (2001). According to Guennoc *et al.* (1994), the CMA represents a body with strong magnetization, induced either by shallow intrusions (6–10 km) or by the combination of a shallow Moho (17–15 km) and intrusions at depths between 11 and 14 km. Those intrusions would be located under the shallow detachment observed by Mauffret & Gennesseaux (1989) and Mauffret *et al.* (2001), in the Palaeozoic basement under the Rascasse horst, because the reflector associated to this structure is continuous (**Fig. 3C**). These authors suggested, by analogy with gravity anomalies along the Pyrenean belt and Mediterranean margins, that the intrusions resulted from two phases of magmatic intrusions into the continental crust. Intrusions of the first phase (Triassic or Early Cretaceous) occurred at depth, near the base of the continental crust. Indeed, Triassic and Cretaceous intrusions in the Pyrenees have similar magnetic susceptibility values (Azambre & Pozzi, 1982). Intrusions of the second phase occurred during Cenozoic extension, consistent with transtensional motions along major NW-SE-trending structures (CTZ and NBTZ), as a leaky transform described in the North Balearic Islands (Mauffret *et al.*, 1992).

241

242 **3. Geophysical data, processing and mapping**

243 For this study, we compiled gravimetric and magnetic data covering most of the GoL area and
244 we then established a complete Bouguer anomaly map (**Fig. 4**) and a reduced-to-the-pole (RTP)
245 magnetic anomaly map (**Fig. 5**), respectively. To constrain the geophysical models, we used some
246 available interpreted seismic sections across the GoL margin and also took into account the geological
247 formations outcropping along the coastline and those sampled by oil exploration wells offshore.

248 ***3.1. Gravimetric data and the Bouguer anomaly map***

249 The gravimetric data compilation includes offshore and onshore data. For the offshore domain,
250 Compagnie Générale de Géophysique (CGG) seafloor gravity data (1966), data from several marine
251 campaigns archived at IFREMER-SISMER, and an Elf-Explo campaign of 1996 allowed us to cover
252 the entire GoL margin. The onshore domain was covered by ground surveys archived in the Banque
253 Gravimétrique de la France (Martelet *et al.*, 2009) for French territory and in the International
254 Gravimetric Bureau database (http://bgi.obs-mip.fr/) for Spain.

255 The combined gravity dataset was carefully reprocessed to align all data with the IGSN71–
256 Hayford 1930 gravity reference system. State-of-the-art gravity data reduction was performed,
257 including free-air and Bouguer slab reduction in which a Bouguer reference density of 2.3 g/cm^3 was
258 used, considering that most data points are located above sedimentary basins. Terrain corrections were
259 computed using a procedure after Martelet *et al.* (2002). Topographic and bathymetric datasets used
260 for free air and Bouguer corrections were made using the IGN digital terrain model topographic
261 dataset (250 m resolution) onshore and the EMODnet bathymetric grid (200 m resolution) offshore
262 (http://www.emodnet-bathymetry.eu). Terrain corrections were computed from 200 m to 10 km
263 around the gravity stations, using topographic grids resampled every 200 m, and from 10 km to 167
264 km using topographic grids resampled every 1 km.

265 Offshore gravity data were reduced, first by trimming the data from different marine campaigns
266 in order to reduce navigation noise and homogenize data sampling. Instrumental drift was reduced
267 using traditional adjustments at profile intersections, first for each survey and then between different
268 surveys, considering the Elf Explo 1996 cruise as the reference. The CGG 1966 seafloor gravity data

was upward-continued to the sea surface before being merged with other datasets. The resulting dataset was finally converted to a 1-km regular grid using a minimum curvature algorithm.

The complete Bouguer anomaly map (**Fig. 4**) incorporates all the density contrasts below the topography. Anomalies range from –264 to +194 mGal and display a regional gravity gradient in which anomalies are mostly negative onshore and positive offshore, highlighting the land-sea transition. At first glance, some gravity anomalies appear to correspond to major geological structures, such as the Nîmes fault.

3.2. Magnetic data and the magnetic anomaly map

The airborne magnetic dataset was acquired in 1965 by CGG using a CSF magnetometer and a Toran positioning system flown at a constant altitude of 900 m above sea level. Magnetic data were collected along flight lines spaced 3 km apart in the NW-SE direction and 12 km apart in the perpendicular direction. After reduction of diurnal variations of the magnetic field, data were interpolated on a 1000-m regular grid using bidirectional gridding. The operator originally applied a regional correction of +2.8 nT/km along the SE-NW flight lines and –0.3 nT/km along the SW-NE lines. We back-corrected this regional trend and adopted a standard regional magnetic reduction based on the International Geomagnetic Reference Field (IGRF) for the date of the survey. Next, a state-of-the-art reduction to the pole (RTP) filter was applied to the dataset, relocating the anomalies directly above their sources, to improve the interpretation of magnetic source locations relative to geologic features. The resulting RTP magnetic anomaly map (**Fig. 5**) displays geomagnetic field strengths ranging from 2950 to 3200 nT. Despite the removal of the long-wavelength IGRF, a SW-NE gradient is apparent. Various rather large magnetic anomalies are observed along the coast line and onshore in figure 5. These seem related to onshore tectonics/structures as the Pyrenean belt or the Nîmes fault for example. The largest magnetic anomaly observed is the CMA. Because of its amplitude, trend and location, and because we cannot associate it to known tectonics features, unlike the other anomalies, we decided to aim our study to understand the CMA and the anomaly B.

4. 2D geophysical modelling

Gravimetric and magnetic modelling consists of simulating the distributions of density and magnetic susceptibility that best explain the measured geophysical data. In practice, after positioning the geophysical profiles to be modelled, a 2D geological model is created. Each layer of this model is assigned values of density and magnetic susceptibility to allow the computation of modelled gravimetric and magnetic effects. Displaying the measured Bouguer anomaly and RTP magnetic anomaly data along specific profiles allows a direct visual comparison of observed and modelled geophysical effects.

Many models were tested by modifying the geometry of the starting model to best match the geophysical responses of the model with the observed geophysical data. Different structures and bodies can equally well explain the measured signal. Therefore, it is necessary to introduce as many structural constraints and as much field information as possible during the modelling process to reduce the inherent uncertainty of the method. In this process, knowledge of the geological context is important to test the most meaningful hypotheses. The shape, wavelength and intensity of gravimetric and magnetic anomalies allow to address the size, intensity and depth of density contrasts. In our investigation of the CMA and anomaly B, we modelled two perpendicular cross-sections, M1 and M2 (**Fig. 2** and **Fig. 5**).

Cross-section M1 oriented NW-SE, crosses the whole GoL margin from the inner continental shelf to the abyssal plain. From the unthinned continental domain to the oceanic domain, it goes along the CMA's axis of higher amplitude and goes through the Catalan basin. This cross-section is parallel and close to (~15 km east) the SARDINIA seismic profile, which doesn't cross the higher values of the CMA (lower values at the end of extension).

Cross-section M2 oriented SW-NE, intersects the CMA, anomaly B and the SARDINIA and ECORS seismic profiles. It runs from Cap de Creus (Pyrenean crust) to Marseille (Provençal crust), along the present shelf break.

4.1. The 2D geometric model

Our geophysical cross-sections were computed from a 2D geometric model containing multiple layers, each characterized by specific densities and magnetic susceptibilities. Remanent magnetization

was not considered because no strong remanent anomalies appear in the RTP map (**Fig. 5**). The layer-cake model (**Fig. 6**) extends through the lithosphere to 50 km depth and extends laterally to infinity in order to avoid edge effects. Because our model integrates deep density contrasts down to the Moho, the complete Bouguer anomaly is used rather than a residual Bouguer anomaly more appropriate for relatively superficial layers. Our initial model is defined by the following five layers:

- The water layer is defined by zero elevation (top) and the EMODnet bathymetry grid (base).
- The Tertiary sedimentary cover encompasses synrift and postrift formations, with mainly detrital lithologies (Gorini *et al.*, 1993; Guennoc *et al.*, 2000). The base of this cover is derived from interpreted seismic data (Couëffe *et al.*, 2016). This layer includes three sublayers that gradually increase in density with depth in order to take into account diagenetic effects. From top to bottom, the density values are 2350 kg/m^3, 2400 kg/m^3 and 2600 kg/m^3 based on the gravimetric cross-sections of Guennoc *et al.* (1994) and common values from Berndt *et al.* (2001) and Keen *et al.* (2018).
- The upper continental crust is delimited on the basis of the SARDINIA seismic velocity model (Moulin *et al.*, 2015; **Fig. 3**A), and its density (2750 kg/m^3) is adapted from the three-layered global model CRUST1.0 (Laske *et al.*, 2012). For 2D modelling, the Paleozoic and Mesozoic prerift formations are integrated in this layer because their density (2700 kg/m^3, Guennoc *et al.*, 1994) is similar, their thickness is negligible in the CMA area and their extent is not well mapped.
- The lower continental crust is based on the interpreted ECORS seismic profile (Séranne, 1999; **Fig. 3**B) and the seismic interface of Diaz *et al.* (2018). Its density, also adapted from CRUST1.0, is set at 2950 kg/m^3.
- The lithospheric mantle is defined by the Moho geometry, compiled from many authors (e.g. Chamot-Rooke et al , 1999; Gallart *et al.*, 2001; Mauffret *et al.*, 2001; Nercessian *et al.*, 2001; Gailler *et al.*, 2009; Diaz *et al.*, 2018; Wehr *et al.*, 2018) and from CRUST1.0 in otherwise unconstrained areas. Its density of 3360 kg/m^3 is a conventional value for the average upper mantle (Braun & Beaumont, 1989).

The boundaries between the continental (I), transitional (II) and oceanic (III) domains are derived from the interpreted seismic profiles (Séranne, 1999; Gailler *et al.*, 2009; Bache *et al.*, 2010; Moulin *et al.*, 2015). The transitional (II) and oceanic (III) domains are outside the area where high-resolution data from the 1965 aeromagnetic survey are available, thus no hypothesis concerning their crustal magnetization could be tested. Therefore, we set their magnetic susceptibility to null as it did not affect the calculated magnetic signal. The crust of the transitional domain is characterized by a velocity between those of the lower crust and mantle (Moulin *et al.*, 2015), and accordingly its density should be in between mantle and lower crust densities. We applied a density of 2850 kg/m^3 (comparable to Elo, 1997) for the oceanic crust of domain III.

The sedimentary cover, upper and lower continental crusts and the mantle are considered to be nonmagnetic in our models. Crustal geometry and domain limits provided by the SARDINIA and ECORS seismic profiles (**Fig. 3**) and the geological formations outcropping along the coastline and sampled by offshore wells (**Fig. 2**) were also taken into account.

Note that in the following, the geometries of the water layer (bathymetry values, Fig. 2) and the sedimentary cover (Fig. 2, 3; Gorini 1993; Guennoc et al., 2000; Bache et al., 2010; Coueffé *et al.*, 2016) were not modified as they are closely constrained by data whereas the other limits were adjusted to best fit the data.

4.2. Geological hypotheses

Considering the lobate shape of the CMA, the corresponding magnetized body must consist of two separate parts to coincide with the structure suggested by the magnetic data (**Fig. 5**). Considering the strong intensity of the CMA, the magnetic body must either be very thick or have an extremely high magnetic susceptibility. Because of the long wavelength of this anomaly, modelling shows that the source body must be deeper than 5 km, thus below the sedimentary cover. The absence of any gravimetric feature over the CMA (**Fig. 4**) attests that the magnetized body must have a density close to its surroundings.

To reduce the range of possible models for the CMA, we tested seven geological hypotheses (H1 through H7 in **Table 1**) consistent with the geologic and geodynamic context seen in other

continental margins with magnetic anomalies. These involved four basic sources for the geophysical signal of the CMA:

- A basaltic body (H1 and H3). Basaltic intrusions have been described as volcanic seamounts at the top of the substratum in surrounding areas (Valencia Trough from Maillard, 1993 and Mauffret *et al.*, 1995; Corsica margin from Réhault *et al.*, 2012).
- A gabbroic body (H4 and H5). Gabbroic intrusions, mafic contamination and mafic underplating have been described on the Vöring volcanic continental margin (Berndt *et al.*, 2001) and the Iberia nonvolcanic continental margin (Neres *et al.*, 2018), and gabbroic sills and dykes have been described in the upper continental crust of other margins (e.g. Northern Red Sea margin; Ligi *et al.*, 2018).
- A mix of basalt and gabbro bodies (H2), as described in the Newfoundland-Iberia conjugate rift system (Bronner *et al.*, 2011).
- A body of serpentinized mantle (H6 and H7), as described in the central Labrador margin (Keen *et al.*, 2018).

Due to the size and intensity of the CMA, magnetic susceptibilities were initially based on published studies and then modified during modelling. For each hypothesis, the density was fixed, whereas the shape and magnetic susceptibility of the modelled body were adjusted over several iterations, taking into account the geological possibilities, to properly fit the model to the observed geophysical data along the two cross-sections.

5. Modelling results and key observations

The CMA is 50 km long and 20 km wide. It has a magnetic amplitude as great as 3450 nT (**Fig. 5**). This anomaly lies entirely within domain I, which is characterized by thinned continental crust under the continental slope (**Fig. 2**). The observed magnetic and gravimetric signals along cross-sections M1 and M2 are shown in **Fig. 7**.

5.1. Selection of working hypotheses best fitting the geophysical signal

For each proposed hypothesis, the intensity and shape of the calculated magnetic signal could be adjusted to match the observed magnetic signal, except for H1, which could not quite be made to fit

405 the curve. Concerning the gravimetric data, the resulting magnetic bodies led to a mass excess for H1
406 to H4 and a mass deficit for H6 and H7 (**Table 1**).

407 The presence of a high-velocity body in the thinned continental domain on the SARDINIA
408 seismic profile (domain I, **Fig. 3**) favours the three hypotheses that include a dense body beneath the
409 thinned continental crust (H2, H4 and H5, **Table 1**).

410 We ruled out H1 and H2 because neither volcanic seamounts nor sills/dykes have been
411 described in the seismic profiles or sampled in the area of the CMA (Rascasse well; Gorini *et al.*,
412 1993; Mauffret *et al.*, 1995; Guennoc *et al.*, 2000). Moreover, the continuity of the detachments in the
413 Paleozoic basement there weighs against the presence of magmatic bodies above (Guennoc *et al.*,
414 1994).

415 Hypotheses H6 and H7, involving a body of serpentinized mantle, were carefully tested. But the
416 degree of serpentinization must be quite high to obtain the intensity of the CMA. Maffione *et al.*
417 (2014) measured magnetic susceptibility values greater than 0.02 SI for a degree of serpentinization
418 higher than 60%, which would imply a density lower than 2540 kg/m^3 (Miller & Christensen, 1997).
419 The shape of the CMA's magnetic signal thus could be explained only by a high degree of
420 serpentinization over a large volume, which is inconsistent with the geological context, leading us to
421 dismiss H6 and H7. Moreover, those hypotheses led to a mass deficit inconsistent with the gravimetric
422 signal (**Table 1**).

423 After many different tests, the most successful hypothesis was H5, which implies the occurrence
424 of mafic rocks of gabbroic type at depth (**Table 1** and **Fig. 7**). These igneous rocks may underplate the
425 continental crust and infiltrate the lower continental crust. The petrophysical parameters of hypothesis
426 H5 allowed us to adopt model geometries that matched the gravimetric and magnetic observations
427 better than the other hypotheses. The overall geometry and location of the large-scale magnetic body
428 remains similar regardless of the different lithologies. Hereafter the magnetic body generating the
429 CMA is called the Catalan body.

5.2. Proposed 2D geophysical model

Our model for cross-sections M1 and M2 (**Fig. 7**), described below, were obtained using hypothesis H5. These sections are considered here as the final result of the modelling, as they best match the magnetic and gravimetric data and fulfil reasonable geological hypotheses.

5.2.1. Section M1

Section M1 extends perpendicular to the GoL margin from the continental domain onshore to the deep oceanic domain offshore (**Fig. 2**). In agreement with the SARDINIA and ECORS seismic profiles, the Cenozoic sedimentary cover thickens from negligible at the coastline to 9 km thick at the outer edge of domain I. The boundary between the upper and lower continental crust is at around 13 km depth, in accordance with the nearby SARDINIA seismic profile.

The regional gravity signature along this section fits a significant crustal thinning in two necking zones that are linked to a rise in the mantle from 30 km to about 10 km deep over a horizontal distance of 180 km. The first necking zone is under the western part of the Graben Central, i.e. the Catalan basin, and the second one is under the continental slope of the GoL margin. Under the Catalan basin, the gravity mass deficit imposed by the 6-km-thick sedimentary infill is compensated by a rise in the Moho nearly to 15 km depth over a horizontal distance of 40 km.

Under the Rascasse horst, the Moho is deeper and thus a thicker crustal block is present in that area (around 20 km). It is composed of upper continental crust (less than 10 km thick) and the Catalan body. The lateral extent of the Catalan body corresponds to the width of the CMA.

The Catalan body is located at the top of the mantle in the necking area of the GoL margin (**Fig. 7**). Its fit with the CMA and gravity values indicates respectively that it must be a highly magnetized body with low density contrast with its surroundings. In order to better approach the most probable field conditions, we created a vertical gradient of density and magnetic susceptibility by dividing the Catalan body into three distinct bodies (numbered 7, 8 and 9 in **Fig. 7**) with decreasing density and magnetic susceptibility from bottom to top (see **Table 1**). The lower body is assigned a density typical of gabbro, and the middle and upper bodies have the densities close to the densities assigned to the lower and upper crust, respectively (**Table 1**). The Catalan body under the Rascasse horst coincide

457 with a deepening of the moho and a thickening of the crust. The shallower part of the Catalan body
458 contains two indentations to fit the two lobes of the magnetic high.

459 In the transitional domain (domain II, **Fig. 1**), gravimetric values imply an unusually dense
460 (3100 kg/m^3) and thin (2–3 km) crust between the sedimentary cover (2600 kg/m^3) and the mantle
461 (3360 kg/m^3). This ascribed density corresponds to neither typical lower continental crust (2950
462 kg/m^3) nor unaltered mantle material (3360 kg/m^3). Different hypotheses are made concerning its
463 nature, it could be 1) a hyperextended lower continental crust that is densified by mafic intrusions (e.g.
464 Séranne *et al.*, 1995; Séranne, 1999; Moulin *et al.*, 2005, 2015; Aslanian *et al*, 2009; Jolivet *et al.*,
465 2015); (2) an exhumed serpentinized mantle (Boillot *et al.*, 1980, 1987, 1989; Beslier *et al.*, 1993) or
466 (3) an atypical oceanic crust formed at a very slow spreading rate (e.g. Dick *et al.*, 2003; Klimke *et al.*,
467 2016; Sauter *et al.*, 2016). Strong debates are ongoing between the first two hypotheses. Recent
468 studies demonstrate the occurrence of important volcanic edifices and magmatic crust in the north of
469 the Valencia Basin close to the GoL transitional domain (Jolivet *et al.*, 2019; Maillard et al., 2019).
470 The most plausible hypothesis to us would be the hyperextended lower crust intruded by mafic
471 magmatic product with low magnetic susceptibility. The second hypothesis is possible but it seems
472 difficult to connect an exhumed serpentinized mantle with the recent observed magmatic crust of the
473 Northern Valencia basin. A study and further discussion on the nature of the transitional crust is out of
474 the scope of this paper, interested readers are invited to refer to the quoted papers.

475 To summarize, cross-section M1 presents the geometry of a passive continental margin with
476 significant crustal thinning and a rise in the mantle in the necking zone, with a mafic magmatic
477 underplating and intruding the continental crust.

478 5.2.2. Section M2

479 Section M2 (**Fig. 7**) crosses the continental shelf of the GoL margin (domain I) from the eastern
480 Pyrenees to the Provence area (**Fig. 2**) and cuts through the CMA and anomaly B (**Fig. 5**). It crosses
481 the SARDINIA and ECORS seismic profiles and is located near the recent PYROPE onshore seismic
482 profiles, shown on the western edge of **Fig. 2** (Diaz *et al.*, 2018; Wehr *et al.*, 2018). These seismic data
483 allowed us to constrain the thickness of the Cenozoic sedimentary cover, the boundary between upper
484 and lower continental crust, and the Moho depth.

485 The regional gravity signature along this section fits with a crust that thins from 30 km in the
486 Pyrenees to 12 km in the Catalan zone on one side, and from 35 km in the Provence margin to 12 km
487 in the Catalan zone on the other side. The crustal thinning is greater at a distance of about 80 km east
488 of the Pyrenees, where the corresponding depression is filled by a Tertiary sedimentary cover as thick
489 as 7 km. Note that the continental crust is thicker in the Provence margin than in the eastern Pyrenees.
490 Neither the lower nor the upper crustal layers have the same thicknesses on the opposite sides of the
491 section. On the west (Pyrenean) side, the boundary between the upper and lower crusts rises offshore
492 as the lower crust thins from 10 to 6 km. Inversely on the east (Provence) side, the boundary between
493 the upper and lower crust is fixed at a depth of 14 km, consistently with the SARDINIA and ECORS
494 seismic profiles. The crustal thinning on both sides is linked to a rise in the mantle to a depth of
495 around 20 km. The rise on the western side is smooth and regular (13 km over a horizontal distance of
496 180 km). On the eastern side, the Moho depth (rising by 16 km over 200 km) is based on many
497 published estimates, but it is poorly constrained by a lack of deep seismic data onshore in Provence.

498 The two distinct anomalies (CMA and anomaly B) along the M2 profile represent two different
499 magnetic bodies (**Fig. 7**). On the Pyrenees side, the position of the CMA confines the Catalan body
500 (20 km wide) to the west of the area of the greatest crustal thinning. Anomaly B is located east of the
501 thinnest crust in the GoL margin.

502 On section M2, the CMA is induced by the Catalan body, modelled as three superimposed
503 bodies with different magnetic susceptibilities (7, 8 and 9 in **Fig. 7**; **Table 1**). This body is very
504 narrow (20 km wide) and thick (12 km). The lowest, most intensely magnetized body is 2 km thick,
505 the middle one is 7 km thick and the upper one is 2 km thick. Anomaly B is induced by a small body
506 with the characteristics of magnetic body 7 that is 20 km wide and 2 km thick.

507 In brief, section M2 shows the transition between the Pyrenees and the GoL margin. This
508 transition is characterized by significant crustal thinning and a rise of the mantle, but also by the
509 presence of narrow bodies of mafic rocks flanking the area of maximum thinning.

510

6. Moho topography

6.1. New Moho depth map

A new map of Moho depth (**Fig. 8**) was computed during this study. The base map is an unpublished compilation (G. Martelet, pers. comm.) of published data based on converted seismic interpretations in the GoL (e.g. Séranne, 1999; Gallart *et al.*, 2001; Mauffret *et al.*, 2001; Nercessian *et al.*, 2001; Gailler *et al.*, 2009; Moulin *et al.*, 2015). These data were complemented by Moho depths observed on passive seismic profiles by Diaz *et al.* (2018) in the eastern Pyrenees and by depths derived from the 3D model of Wehr *et al.* (2018), based on seismic interpretation and Bouguer anomaly constraints. The Moho depths calculated from the chosen model of this study were also taken into account. Moho isobaths, based on depths rounded to the nearest kilometre, were inferred from the structural configuration of the margin and the thicknesses of the synrift and postrift sediments (Gorini, 1993; Guennoc *et al.*, 1994; Séranne, 1999; **Fig. 2**). The most recent data were favoured, however, some areas where the connection between different datasets was not straightforward, we did not draw any isobaths especially between the Catalan and Roussillon basins (Fig. 8A, discussion below). The depth-to-Moho digital terrain model (colour field in **Fig. 8A**) is computed by interpolation between the isobaths.

6.2. Impact of the models on Moho topography

In the eastern GoL, the Moho slopes upward evenly towards the toe of the margin. The Moho depth decreases gradually from 25 to 20 km below the continental shelf and more steeply (from 20 to 14 km) below the continental slope and the necking zone. In contrast, the Moho topography is irregular in the western GoL. There, the Moho is shallow, reaching 16 km depth below the Catalan basin in the proximal part of the continental shelf. Because of the lack of data, we can neither validate nor reject a possible structural and geometrical connection between the Catalan and Roussillon basins. In this case, Moho isobaths are not drawn on the western side of the Catalan basin (Fig.8A). Moreover, our models did not allow us to validate or discard the possible presence of the North Pyrenean Fault in the Catalan basin or the Rascasse horst.

Section M1 and the SARDINIA and ECORS profiles parallel to it show significant thinning of the continental crust linked to a rise in the mantle along the whole margin (**Fig. 8B**). Moho isobaths

539 (**Fig. 8**A) indicate a significant landward indentation in the western GoL margin. Here the Moho rises
540 from 30 km deep near the beginning of the hinge zone to less than 15 km in a more proximal area than
541 in the eastern GoL (below the continental shelf), and the Moho rise is steeper in section M1 than in the
542 SARDINIA (15 km to its east) and ECORS profiles (**Fig. 8**B). Section M1 shows that the boundary
543 between domains I and II is located at the same level as interpreted by Moulin *et al.* (2015) on the
544 SARDINIA profile.

545 In the Pyrenees-GoL transition, the Moho rises steeply from 25 to 15 km depth over a horizontal
546 distance of ~50 km northeast of the Cap de Creus (**Fig. 8**A). The map shows an abrupt margin
547 trending NW-SE. This orientation matches those of the CTZ, the shear zones of Cap de Creus and the
548 Figueres-Montgrí basin to its southwest (e.g. Carreras, 2001; Vissers *et al.*, 2016; Monié *et al.*, 2018;
549 Druguet *et al.*, 2018).

550

551 **7. Discussion**

552 The results of our 2D geophysical modelling provide new information on the origin of the CMA
553 and the transition between the Pyrenees and the GoL margin. They are discussed below in relation to
554 the geodynamic context.

555 ***7.1. The Catalan body***

556 Modelling based on gravimetric and magnetic data implies the presence of a large mafic
557 magmatic body below the western GoL margin, called here the Catalan body, and a smaller one to its
558 east corresponding to anomaly B (**Fig. 1** and **Fig. 5** and profile M2 in **Fig. 7**). The Catalan body is
559 approximately 80 km long, 20 km wide, and 12 km thick and is oriented NW-SE. It is located in the
560 necking area of the GoL continental margin, but not in the thinnest continental crust area. Both bodies
561 have magnetic and gravimetric properties consistent with those of gabbroic rocks. Taking into account
562 the geometries and petrophysical characteristics of the models along our two profiles, we interpret the
563 Catalan body as a gabbroic magmatic body that underplates (body 7 in **Fig. 7**) and intrudes the thinned
564 lower and upper continental crust (bodies 8 and 9, respectively). Anomaly B is explained by the
565 presence of a smaller underplating mafic magmatic body (body 7).

566 The setting of the Catalan body can be explained by several hypotheses, proposed on the basis
567 of the regional geodynamic context.
568 One hypothesis is that the Catalan body is a mafic underplating and intruding the thinned
569 continental crust, like those observed on volcanic margins. However, the GoL doesn't show the main
570 features of a typical volcanic margin (Geoffroy *et al.*, 2005): no SDR (seaward-dipping reflector) has
571 been observed in the upper crust and most authors described the GoL as a nonvolcanic continental
572 margin (e.g. Séranne *et al.*, 1995; Séranne, 1999; Moulin *et al.*, 2005, 2015; Aslanian *et al*, 2009;
573 Jolivet *et al.*, 2015). The Catalan body could be the product of basaltic melt intrusions into this margin
574 during the Oligo-Miocene extension and breakup of the continental lithosphere, by analogy to the
575 Northern Red Sea margin (Ligi *et al.*, 2018).
576 A second hypothesis is that the Catalan body is the product of back-arc volcanism along the
577 CTZ, coherent with proposed kinematic reconstructions (Jolivet et al., 2015; Romany et al., in prep;
578 Jolivet *et al.*, 2019) . Indeed, magmatic bodies on the surrounding margins of southeastern France and
579 Corsica formed in the back-arc region of the retreating Apennine slab during the rotation of the
580 Corsica-Sardinia block (Jolivet & Faccenna, 2000; Rehault *et al.*, 2012). Transfer faults, which
581 accommodate different rates of extension, might have localized and constrained the emplacement of
582 these magmatic bodies. Indeed, the Catalan body is in the Catalan transfer zone (CTZ). The CTZ may
583 belong with the North Balearic transfer zone (NBTZ, Fig 1) to the same system, allowing the Corsica-
584 Sardinia block rotation and the opening of the Liguro-Provençal basin (**Fig. 1**).
585 A third hypothesis is that the magmatic material came from the magmatic province of northern
586 Valencia Trough described by Maillard et al. (2019) through the CTZ, which acted as a leaky
587 transform and localized the Catalan magmatic body. Indeed, volcanic and magmatic seamounts are
588 aligned along the transfer zones that segment the Valencia Trough (**Fig. 1**, Maillard *et al.*, 1992). In
589 the north eastern Valencia Trough, Maillard *et al.*, 2019 depicts a volcanic province where magmatic
590 formation can reach a 3 km thickness in a spreading zone above a thin and sheared crust, implying
591 high temperatures and ductile behaviour during rifting. This area is affected by the NBTZ. The Catalan
592 Body may be a magmatic body linked to the Valence magmatic province by the CTZ.

By analogy to the Vøring volcanic transform margin, a fourth hypothesis could be that the magmatic material originated during transtension along a transfer fault (the CTZ in our case). Indeed transtensional motion can open pull-apart basins and lead to crustal thinning that promotes melt production (Berndt *et al.*, 2001; White & McKenzie, 1989; Pedersen & Skogseid, 1989). Berndt *et al.* (2001) referred to such magmatic intrusions as "transform margin highs". They have been reported in multiple transition zones such as East Canada (Reid, 1989), the Exmouth Plateau (Lorenzo *et al.*, 1991; Lorenzo & Vera, 1992), the western Barents Sea margin (Vågnes, 1997) and the Côte d'Ivoire–Ghana margin (Basile *et al.*, 1998). In agreement with this hypothesis, according to Mauffret *et al.* (2001), extension related to transfer activity should not be confused with the normal extension associated with horst and graben structures, suggesting that the Catalan basin could be formed during a pull-apart motion. Moreover, the Moho map shows an abrupt margin trending NW-SE at the East of Cap de Creus (Eastern Pyrenees), similar to the morphology of a transform margin highs.

On the basis of the regional geodynamic context, we propose that the setting-up of the Catalan body was induced by a combination of these events. The slab retreat and the motion along transfer zones during the opening of the Liguro-Provençal Basin lead to a continental crust thinning and induced the production of hot and ductile material in this area. This magma followed the facilitated paths created by the major crustal fault of the CTZ, maybe the fault n°1 described by Mauffret et al (2001) (see fig 2).

7.2. Age of the Catalan body

The question arises as to the history of the tectonic structures around the Catalan body. The NW-SE-trending transfer zones or faults in the area could be reactivated structures inherited from the Pyrenean collision, the Mesozoic rifting or the Hercynian orogeny. Indeed, reactivated Paleozoic and Pyrenean shear zones with similar orientations are found in the Cap de Creus area (e.g. Carreras, 2001; Vissers *et al.*, 2016; Monié *et al.*, 2018; Druguet *et al.*, 2018), and further south the Mesozoic Figueres-Montgrí basin is also oriented NW-SE. Thus we cannot rule out the possibility that the Catalan body was inherited from previous tectonic events. However, two facts weigh against this possibility. Firstly, the orientation of the CMA is parallel and superimposed onto the CTZ which is linked to the opening of the Liguro-Provençal Basin. Secondly, near the Catalan body and on adjacent

and conjugate margins (Valencia and Sardinia respectively), there is the occurrence of Miocene volcanism (Jolivet *et al.*, 2015), induced by the slab retreat of the Apennines (Maillard et al., 2019; Jolivet et al., 2019) dated to 30 Ma (e.g. Auzende et al.,1973; Gattaccecea et al., 2007). On the kinematic reconstruction, the volcanism of the SW Sardinia margin and the northern Valencia basin fits with the Catalan body. Thus we favour an interpretation that involves underplating and intrusion of mafic melt related to the transfer zone motion linked to the opening of the Liguro Provençal basin associated with magmatism caused by back-arc extension.

7.3. The Pyrenees – GoL margin transition

From our new Moho depth map and models we show that the western part of the GoL margin (from SARDINIA profile to the cap de Creus, ~50 km wide) is characterized by a heterogeneous crustal structure (see the M1 and SARDINIA profiles in **Fig. 8**B). The thinned continental domain (domain I) of this area is composed of (i) a thinned to hyper-thinned continental crust (25 to 0 km thick), (ii) a rising mantle below thick Tertiary sedimentary sequences in the Catalan and Cathares basins and (iii) the presence of a mafic magmatic body below the Rascasse horst. This deep structure of the western side of the GoL margin (Cross-section M1 in Fig. 7) is not observed in the eastern part of the GoL margin (ECORS profile in Fig. 8). To the east, crustal necking is in a more distal position, tilted blocks are observed and even the thickness of the synrift deposits are uneven. The western extremity of the GoL margin is bounded by a steep mantle rise at the toe of the Cap de Creus (eastern Pyrenees; ***Fig. 8***A).

We propose that this 50 km wide area is the marker of the CTZ, with many transfer faults as suggested by Mauffret et al. (2001) (fault n°1 on Fig 2). The CTZ could extend further south, according to Mauffret *et al.* (2001) and more recent seismic interpretations in the northern Valencia Trough (Maillard *et al.* 2019; Jolivet *et al.*, 2019).

The CTZ marks the transition from the Eastern Pyrenees to the GoL margin, which is not abrupt but is a wide area. This transition would result from the transtensional motion along the transfer faults of the CTZ and not only be linked to the rifting phase. The CTZ and the NBTZ belong to the same transfer system that allowed the rotation of the Corsica-Sardinia block and the opening of the Liguro-Provençal domain.

649 Even though the Tertiary formation of the Catalan basin, the CTZ and the Catalan magmatic
650 body are supposed to be coeval with the opening of the Liguro-Provençal Basin, we cannot rule out
651 the role of inherited structures from the Hercynian orogeny, Mesozoic rifting and Pyrenean orogeny in
652 explaining the crustal heterogeneity, transfer zones and Moho morphology of the GoL
653

654 **8. Conclusions**

655 To better characterize the transition between the Pyrenees and the Gulf of Lion (GoL) margin, a
656 wide range of available aeromagnetic and gravimetric data have been reprocessed to interpret of the
657 Catalan Magnetic Anomaly (CMA), the major high-amplitude magnetic anomaly of the GoL margin at
658 the foot of the eastern Pyrenees chain. We proceed to compute new RTP magnetic anomaly and
659 Bouguer anomaly maps, model the CMA from gravimetric and magnetic data and create a new Moho
660 depth compilation map.

661 From geophysical modelling along two perpendicular cross-sections, the CMA is interpreted as
662 a mafic magmatic body of significant dimensions (80 × 20 × 12 km), called the Catalan body. This
663 body underplates and intrudes the thinned continental crust in the necking zone of the western part of
664 the GoL margin along a crustal fault of the Catalan Transfer Zone (CTZ). We propose that this
665 magmatism was due to the transtensional motion along the CTZ, induced by the back-arc extension
666 above the retreating Apennine slab and thus produced during the Tertiary rifting phase of the Liguro-
667 Provençal Basin.

668 From the new compilation map of Moho depths, the 50 km-wide zone oriented NW-SE and
669 located in the western part of the GoL margin is attributed to the CTZ. The CTZ marks the transition
670 from the Pyrenean mountain belt to the GoL margin. It is characterized by a heterogeneous crustal
671 structure and Moho geometry: i) In the continental shelf, an important mantle rise is beneath the thick
672 Tertiary Catalan sedimentary basin (western part of the Graben Central); ii) The necking zone is more
673 proximal and steeper than that in the GoL margin at East; iii) The presence of the mafic magmatic
674 body in the thinned continental domain, certainly set up along a NW-SE crustal fault. The CTZ
675 belongs to the same transfer system as the NBTZ that allowed the rotation of the Corsica-Sardinia
676 block and the opening of the Liguro-Provençal domain.

677

678

679 **Acknowledgments:**

680 This study was carried out during the OROGEN project, funded by TOTAL, BRGM, and
681 INSU-CNRS. We thank the OROGEN's community for their helpful discussions. We are thankful for
682 the availability of the data accessible on the European Marine Observation and Data Network
683 Bathymetry portal (http://www.emodnet-bathymetry.eu) for the bathymetric metadata and digital
684 terrain model data products, and also for the BRGM's InfoTerre portal for the new geophysical
685 compilation (the gravimetric and magnetic database).We thank Andrew Alden for his proofreading
686 review, as well as the reviewers for their critical and constructive reviews.

687

688 **References**

689

690 Arthaud, F., Matte, P., 1975. Les décrochements tardi-hercyniens du sud-ouest de l'Europe. Géométrie
691 et essai de reconstitution des conditions de la déformation. Tectonophysics 25(1-2), 139-171.
692 Aslanian, D., Moulin, M., Olivet, J-L., Unternehr, P., Bache, F., Rabineau, M., Matias, L., Nouzé, H.,
693 Klingelhoefer, F., Contrucci, I., Labails, C., 2009. Brazilian and African passive margins of the
694 Central Segment of the South Atlantic Ocean: kinematic constraints. Tectonophysics 468, 98-
695 112.
696 Auzende, J.-M., Bonnin, J., Olivet, J.-L., 1973. The origin of the western Mediterranean basin. J. Geol.
697 Soc., London 129, 607-620.
698 Azambre, B., Pozzi, J.-P., 1982. Etude du magnétisme des roches éruptives de la région d'Arette
699 (Pyrenées atlantiques), préliminaire a l'analyse de l'évolution des contraintes régionales. Bull.
700 Soc. Géol. Fr. 7(2), 255-263.
701 Bache, F., Olivet, J.-L., Gorini, C., Aslanian, D., Labails, C., Rabineau, M., 2010. Evolution of rifted
702 continental margins: The case of the Gulf of Lions (Western Mediterranean Basin). Earth
703 Planet. Sci. Let. 292, 345-356.
704 Bartrina, M.T., Cabrera, L., Jurado, M. J., Guimerà, J., Roca, E., 1992. Evolution of the central
705 Catalan margin of the Valencia trough (western Mediterranean). Tectonophysics 203(1-4), 219-
706 247.
707 Basile, C., Mascle, J., Benkhelil, J., Bouillin, K.-P., 1998. Geodynamic evolution of the Côte d'Ivoire-
708 Ghana Transform Margin: an overview of leg 159 results. Proc. Ocean Drill. Program Sci.
709 Results 159.
710 Bauer, K., Neben, S., Schreckenberger, B., Emmermann, R., Hinz, K., Fechner, N., Weber, K., 2000.
711 Deep structure of the Namibia continental margin as derived from integrated geophysical
712 studies. J. Geophys. Res. 105(B11), 25829-25853.
713 Benedicto, A., Labaume, P., Séguret, M., & Séranne, M. (1996). Low-angle crustal ramp and basin
714 geometry in the Gulf of Lion passive margin: Oligocene-Aquitanian Vistrenque graben, SE
715 France. *Tectonics*, *15*(6), 1192-1212.
716 Bergerat, F., 1987. Stress fields in the European platform at the time of Africa-Eurasia collision.
717 Tectonics 6(2), 99-132.
718 Berndt, C., Mjelde, R., Planke, S., Shimamura, H., Faleide, J.I., 2001. Controls on the tectono-
719 magmatic evolution of a volcanic transform margin: the Voring Transform Margin, NE Atlantic.
720 Mar. Geophys. Res. 22, 133-152.
721 Beslier, M.-O., Ask, M., Boillot, G., 1993. Ocean-continent boundary in the Iberia abyssal plain from
722 multichannel seismic data. Tectonophysics 218, 383-393.

723 Bestani, L., Espurt, N., Lamarche, J., Floquet, M., Philip, J., Bellier, O., Hollender, F., 2015.
724 Structural style and evolution of the Pyrenean-Provence thrust belt, SE France. Bull. Soc. Géol.
725 Fr. 186(4-5), 223-241.
726 Boillot, G., Féraud, G., Recq, M., Girardeau, J., 1989. "Undercrusting" by serpentinite beneath rifted
727 margins: the examples of the west Galicia margin (Spain). Nature 341, 523-525.
728 Boillot, G., Grimaud, S., Mauffret, A., Mougenot, A., Kornbropst, J., Mergoil-Daniel, J., Torrent, G.,
729 1980. Ocean-continent boundary off the Iberian margin: serpentinite diapir west of the Galicia
730 Bank. Earth Planet. Sci. Lett. 48, 23-34.
731 Boillot, G., Winterer, E.L., Meyer, A.W., 1987. Ocean Drilling Program. In: G. Boillot, E.L. Winterer
732 and A.W. Meyer, Eds, Proc. Ocean Drill. Progr., Init. Repts, 103, 663pp. – College Sation, TX:
733 Ocean Drilling Program.
734 Braun, J., Beaumont, C., 1989. A physical explanation of the relation between flank uplifts and the
735 breakup unconformity at rifted continental margins. Geology 17(8), 760-764.
736 Bridges, D., Mickus, K., Gao, S., Abdelsalam, M., Alemu, A., 2012. Magnetic stripes of a transitional
737 continental rift in Afar. Geology 40(3), 203-206.
738 Bronner, A., Sauter, D., Manatschal, G., Péron-Pinvidic, G., Munschy, M., 2011. Magmatic breakup
739 as an explanation for magnetic anomalies at magma-poor rifted margins. Nature Geosc., 4(8),
740 549.
741 Buck, W.R., 2006. The role of magma in the development of the Afro-Arabian Rift System. Geol.
742 Soc., London, Spec. Publ. 259(1), 43-54.
743 Carreras, J., 2001. Zooming on Northern Cap de Creus shear zones. J. Struct. Geol. 23(9), 1457-1486.
744 Carreras, J., Druguet, E., Griera, A., Soldevila, J., 2004. Strain and deformation history in a
745 syntectonic pluton. The case of the Roses granodiorite (Cap de Creus, Eastern Pyrenees). Geol.
746 Soc., London, Spec. Publ. 224(1), 307-319.
747 Chamot-Rooke, N., Gaulier, J. M., Jestin, F., 1999. Constraints on Moho depth and crustal thickness in
748 the Liguro-Provençal basin from a 3D gravity inversion: geodynamic implications. Geol. Soc.,
749 London, Spec. Publ. 156(1), 37-61.
750 Chelalou, R., Nalpas, T., Bousquet, R., Prevost, M., Lahfid, A., Poujol, M., Ballard, J.F., 2016. New
751 sedimentological, structural and paleo-thermicity data in the Boucheville Basin (eastern North
752 Pyrenean Zone, France). C. R. Geoscience 348(3-4), 312-321.
753 Chevrot, S., Sylvander, M., Diaz, J., Martin, R., Mouthereau, F., Manatschal, G., Masini, E., Calassou,
754 S., Grimaud, F., Pauchet, H., Ruiz, M., 2018. The non-cylindrical crustal architecture of the
755 Pyrenees. Scientific reports 8(1), 9591. DOI:10.1038/s41598-018-27889-x
756 Choukroune, P., Mattauer, M., 1978. Tectonique des plaques et Pyrénees; sur le fonctionnement de la
757 faille transformante nord-pyrénéenne; comparaisons avec des modèles actuels. Bull. Soc. Géol.
758 Fr. 7(5), 689-700.

759 Choukroune, P., Seguret, M., Galdeano, A., 1973. Caractéristiques et évolution structurale des
760 Pyrénées. Un modèle de relations entre zone orogénique et mouvement des plaques. Bull. Soc.
761 Géol. Fr. S7-XV (5-6), 600-611.
762 Clerc, C., Lahfid, A., Monié, P., Lagabrielle, Y., Chopin, C., Poujol, M., de St Blanquat, M., 2015.
763 High-temperature metamorphism during extreme thinning of the continental crust: a reappraisal
764 of the North Pyrenean passive paleomargin. Solid Earth 6, 643-668.
765 Couëffé, R., Tourlière, B., Lasseur, E., Bauer, H., Beccaletto, L., Bialkowski, A., Briais, J., Capar, L.,
766 Paquet, F., Serrano, O., Thinon, I., 2016. Géométrie des bassins cénozoïques métropolitains :
767 premier aperçu fourni par la carte des épaisseurs de leur remplissage sédimentaire (projet
768 METROCENE). 25ème Réunion des Sciences de la Terre, 24-28 octobre 2016, Caen, Livre des
769 Résumés, pp. 64.
770 Diaz, J., Vergés, J., Chevrot, S., Antonio-Vigil, A., Ruiz, M., Sylvander, M., Gallart, J., 2018.
771 Mapping the crustal structure beneath the Eastern Pyrenees. Tectonophysics 744, 296-309.
772 Dick, H.J., Lin, J., Schouten, H., 2003. An ultraslow-spreading class of ocean ridge. Nature,
773 426(6965), 405.
774 Druguet, E., 2001. Development of high thermal gradients by coeval transpression and magmatism
775 during the Variscan orogeny: insights from the Cap de Creus (Eastern Pyrenees).
776 Tectonophysics 332(1-2), 275-293.
777 Druguet, E., Carreras, J., Mezger, J.E., 2018. Discussion on 'Middle Jurassic shear zones at Cap de
778 Creus (eastern Pyrenees, Spain): a record of pre-drift extension of the Piemonte–Ligurian
779 Ocean?' *Journal of the Geological Society, London*, 174, 289-300. J. Geol. Soc. 175(1), 187-
780 188.
781 Dunlop, D. J., Prévot, M., 1982. Magnetic properties and opaque mineralogy of drilled submarine
782 intrusive rocks. Geophys. J. Int. 69(3), 763-802.
783 Elo, S., 1997. Interpretations of the gravity anomaly map of Finland. Geophysica 33(1), 51-80.
784 Fournier, F., Tassy, A., Thinon, I., Münch, P., Cornée, J. J., Borgomano, J., Guennoc, P., 2016. Pre-
785 Pliocene tectonostratigraphic framework of the Provence continental shelf (eastern Gulf of Lion,
786 SE France). Bull. Soc. Géol. Fr. 187(4-5), 187-215.
787 Gailler, A., Klingelhoefer, F., Olivet, J. L., Aslanian, D., Technical, O.B.S., 2009. Crustal structure of
788 a young margin pair: new results across the Liguro–Provencal Basin from wide-angle seismic
789 tomography. Earth Planet. Sci. Let. 286(1-2), 333-345.
790 Galdeano, A., Rossignol, J.-C., 1977. Contribution de l'aéromagnétisme à l'étude du Golfe de Valence
791 (Méditerranée Occidentale). Earth Planet. Sci. Let. 34(1), 85-99.
792 Gallart, J., Diaz, J., Nercessian, A., Mauffret, A., Dos Reis, T., 2001. The eastern end of the Pyrenees:
793 Seismic features at the transition to the NW Mediterranean. Geophys. Res. Lett. 28, 2277-2280.

794 Gattacceca, J., Deino, A., Rizzo, R., Jones, D. S., Henry, B., Beaudoin, B., Vadeboin, F., 2007.
795 Miocene rotation of Sardinia: New paleomagnetic and geochronological constraints and
796 geodynamic implications. Earth Planet. Sci. Let. 258(3-4), 359-377.
797 Geoffroy, L., 2005. Volcanic passive margins. Comptes Rendus Geoscience 337(16), 1395-1408.
798 Geoffroy, L., Burov, E. B., & Werner, P. (2015). Volcanic passive margins: another way to break up
799 continents. *Scientific Reports*, *5*, 14828.
800 Gorini, C., 1993. Géodynamique d'une marge passive : le Golfe du Lion (Méditerranée occidentale).
801 Thèse de doctorat, Université Paul Sabatier, Toulouse, 256 pp.
802 Gorini, C., Le Marrec, A., Mauffret, A., 1993. Contribution to the structural and sedimentary history
803 of the Gulf of Lions (western Mediterranean), form the ECORS profiles, industrial seismic
804 profiles and well data. Bull. Soc. Géol. Fr. 164(3), 353-363.
805 Gorini, C., Mauffret, A., Guennoc, P., Le Marrec, A., 1994. Structure of the Gulf of Lions
806 (northwestern Mediterranean Sea): A review. In: Hydrocarbon and Petroleum Geology of
807 France (pp. 223-243). Springer, Berlin, Heidelberg.
808 Granado, P., Urgeles, R., Sàbat, F., Albert-Villanueva, E., Roca, E., Muñoz, J.A., Gambini, R., 2016.
809 Geodynamical framework and hydrocarbon plays of a salt giant: the NW Mediterranean Basin.
810 Petroleum Geoscience 22(4), 309-321.
811 Gueguen, E., Doglioni, C., Fernandez, M., 1998. On the post-25 Ma geodynamic evolution of the
812 western Mediterranean. Tectonophysics 298, p. 259-269.
813 Guennoc, P, Debeglia, N, Gorini, C, Le Marrec, A, Mauffret, A., 1994. Anatomie d'une marge passive
814 jeune (Golfe du Lion - Sud France): apports des données géophysiques. Bulletin des Centres de
815 Recherches Exploration-Production Elf Aquitaine 18(1), 33-57.
816 Guennoc, P., Gorini, C., Mauffret, A., 2000. Histoire géologique du Golfe du Lion et cartographie du
817 rift oligo-aquitanien et de la surface messinienne. Géol. Fr. 3, 67-97.
818 Jolivet, L., Faccenna, C., 2000. Mediterranean extension and the Africa-Eurasia collision. Tectonics
819 19(6), 1095-1106.
820 Jolivet, L., Augier, R., Robin, C., Suc, J.-P., Rouchy, J.-M., 2006. Lithospheric-scale geodynamic
821 context of the Messinian salinity crisis. Sed. Geol. 188, 9-33.
822 Jolivet, L., Gorini, C., Smit, J., Leroy, S., 2015. Continental breakup and the dynamics of rifting in
823 back-arc basins: The Gulf of Lion margin. Tectonics 34(4), 662-679.
824 Jolivet L., Romagny A., Gorini C., Maillard A., Canva A., Thinon I., Coueffé R. and Peyrefitte A.,
825 2019. Post-orogenic evolution of Pyrenees and Liguro-Provençal rifting, the role of mantle flow.
826 Poster. Geophysical Research Abstracts Vol. 21, EGU2019-4033-1.
827 Kearey, P., Brooks, M., Hill, I., 2002. An introduction to Geophysical Exploration. Third edition.
828 Blackwell Science Ltd, 262 p.
829 Keen, C.E., Dickie, K., Dafoe, L.T., 2018. Structural characteristics of the ocean-continent transition
830 along the rifted continental margin, offshore central Labrador. Mar. Petrol. Geol. 89, 443-463.

831 Klimke, J., Franke, D., Gaedicke, C., Schreckenberger, B., Schnabel, M., Stollhofen, H., Chaheire, M.,
832 2016. How to identify oceanic crust - Evidence for a complex break-up in the Mozambique
833 Channel, off East Africa. Tectonophysics 693, 436-452.
834 Lagabrielle, Y., Bodinier, J.-L., 2008. Submarine reworking of exhumed subcontinental mantle rocks:
835 field evidence from the Lherz peridotites, French Pyrenees. Terra Nova 20(1), 11-21.
836 Lagabrielle, Y., Labaume, P., de Saint Blanquat, M., 2010. Mantle exhumation, crustal denudation,
837 and gravity tectonics during Cretaceous rifting in the Pyrenean realm (SW Europe): Insights
838 from the geological setting of the lherzolite bodies. Tectonics 29(4), TC4012
839 doi:10.1029/2009TC002588
840 Laske, G., Masters, G., Ma, Z., Pasyanos, M.E., 2012. CRUST1. 0: An updated global model of
841 Earth's crust. Geophys. Res. Abs. 14, 3743.
842 Lefebvre, D., 1981. Evolution morphologique et structurale du Golfe du Lion. Essai de traitement
843 statistique des données. Thèse de 3ème cycle, Paris VI, 163 pp.
844 Ligi, M., Bonatti, E., Bosworth, W., Cai, Y., Cipriani, A., Palmiotto, C., Seyler, M., 2018. Birth of an
845 ocean in the Red Sea: Oceanic-type basaltic melt intrusions precede continental rupture.
846 Gondwana Res. 54, 150-160.
847 Liotard, J. M., Maluski, H., & Dautria, J. M., 1991. Un Episode magmatique alcalin d'âge éocène en
848 Languedoc; la brèche volcanique de la montagne de la Moure (Hérault). *Bulletin de la Société*
849 *Géologique de France*, *162*(6), 1067-1074.
850 Lorenzo, J. M. Vera, E.E., 1992. Thermal uplift and erosion across the continent-ocean transform
851 boundary of the southern Exmouth Plateau. Earth Planet. Sci. Lett. 108, 79-92.
852 Lorenzo, J. M., Mutter, J. C., Larson, R. L., Northwest Australia Study Group., 1991. Development of
853 the continent-ocean transform boundary of the southern Exmouth Plateau. Geology 19, 843-846.
854 Maffione, M., Morris, A., Plümper, O., Van Hinsbergen, D.J.J., 2014. Magnetic properties of variably
855 serpentinized peridotites and their implication for the evolution of oceanic core complexes,
856 Geochem. Geophys. Geosyst. 15, 923-944. doi: 10.1002/2013GC004993.
857 Maillard, A., Mauffret, A., Watts, A. B., Torné, M., Pascal, G., Buhl, P., & Pinet, B., 1992. Tertiary
858 sedimentary history and structure of the Valencia trough (western
859 Mediterranean). *Tectonophysics*, *203*(1-4), 57-75.
860 Maillard, A., 1993. Structure et riftogenèse du Golfe de Valence (Méditerranée occidentale). Thèse de
861 doctorat, Université Paris VI, 284 pp.
862 Maillard, A., Mauffret, A., 1993. Structure et volcanisme de la fosse de Valence (Méditerranée nord-
863 occidentale). Bull. Soc. Géol. Fr. 164(3), 365-383.
864 Maillard, A., Mauffret, A., 1999. Crustal structure and riftogenesis of the Valencia Trough (north-
865 western Mediterranean Sea). Basin Res. 11(4), 357-379.

Maillard, A., Gaullier, V., Vendeville, B. C., & Odonne, F. 2003. Influence of differential compaction above basement steps on salt tectonics in the Ligurian-Provençal Basin, northwest Mediterranean. *Marine and Petroleum Geology*, *20*(1), 13-27.

Maillard A., Jolivet L., Thinon I., Lofi J., Coueffé R. and Canva A. Accepted in 2019. Transfer Faults and associated volcanic province in the Valencia Basin: consequences on crustal thinning. Marine and Petroleum Geology.

Martelet, G., Debéglia, N., Truffert, C., 2002. Homogénéisation et validation des corrections de terrain gravimétriques jusqu'à la distance de 167 km sur l'ensemble de la France, C. R. Geoscience 334, 449-454.

Martelet, G., Pajot, G., Debeglia, N., 2009. Nouvelle carte gravimétrique de la France; RCGF09–Réseau et Carte Gravimétrique de la France, 2009. Rapport BRGM/RP-57908-FR, 77 pp.

Marti, J., Mitjavila, J., Roca, E., Aparicio, A., 1992. Cenozoic magmatism of the Valencia trough (western Mediterranean): Relationship between structural evolution and volcanism. Tectonophysics 203(1-4), 145-165. Doi: https://doi.org/10.1016/0040-1951(92)90221-Q

Mascle, A., Vially, R., Deville, E., Biju-Duval, B., Roy, J.-P., 1996. The petroleum evaluation of a tectonically complex area: the western margin of the Southeast Basin (France). Mar. Petrol. Geol. 13, 941-961.

Mauffret, A., Genneseaux, M., 1989. Compression, décrochement et distension sur le pourtour méditerraneéen nord-occidental. C. R. Acad. Sci. Paris 308, 961-967.

Mauffret, A., Maillard, A., Pascal, G., Torné, M., Buhl, P., Pinet, B., 1992. Long-listening multichannel seismic profiles in the Valencia trough (Valsis 2) and the Gulf of Lions (ECORS): a comparison. Tectonophysics 203(1-4), 285-304.

Mauffret, A., Pascal, G., Maillard, A., Gorini, C., 1995. Tectonics and deep structure of the north-western Mediterranean Basin. Mar. Petrol. Geol. 12(6), 645-666.

Mauffret, A. & Gorini, C., 1996. Structural style and geodynamic evolution of Camargue and Western Provencal basin, southeastern France. Tectonics 15, 356-375. doi:10.1029/95TC02407.

Mauffret, A., Durand de Grossouvre, B., Tadeu dos Reis, A., Gorini, C., Nercessian, A., 2001. Structural geometry in the eastern Pyrenees and western Gulf of Lion (Western Mediterranean). J. Struct. Geol. 23, 1701-1726.

Miller, D.J., Christensen, N.I., 1997. Seismic velocities of lower crustal and upper mantle rocks from the slow-spreading mid-Atlantic ridge, South of the Kane Transform zone (MARK), in Proceeding of the Ocean Drilling Program, Scientific Results, vol. 153, 437–454, Ocean Drill. Program, College Station, Tex., doi:10.2973/odp.proc.sr.153.043.1997.

Monié, P., Oliot, E., Faucher, A., Allard, M., 2018. Age Eocène $^{40}Ar/^{39}Ar$ des zones de cisaillement de basse température dans la péninsule du Cap de Creus (NW Espagne). Conséquences géodynamiques. Talk. Congres Réunion des Sciences de la Terre RST 26th edition. Lille.

902 Abstract p.234. https://rst2018-
903 lille.sciencesconf.org/data/book_rst2018_lille_fr_final_DEF_web.pdf
904 Moulin, M., Aslanian, D., Olivet, J.-L., Contrucci, I., Matias, L., Géli, L., Klingelhoefer, F., Nouzé,
905 H., Réhault, J.-P., Unternehr, P., 2005. Geological constraints on the evolution of the Angolan
906 margin based on reflection and refraction seismic data ZaïAngo project. Geophys. J. Int. 162,
907 793-810.
908 Moulin, M., Klingelhoefer, F., Afilhado, A., Aslanian, D., Schnurle, P., Nouzé, H., Feld, A., 2015.
909 Deep crustal structure across a young passive margin from wide-angle and reflection seismic
910 data (The SARDINIA Experiment)–I. Gulf of Lion's margin. Bull. Soc. Géol. Fr. 186(4-5),
911 309-330.
912 Nercessian, A., Mauffret, A., Dos Reis, A. T., Vidal, R., Gallart, J., Diaz, J., 2001. Deep reflection
913 seismic images of the crustal thinning in the eastern Pyrenees and western Gulf of Lion. J.
914 Geodynamics 31(2), 211-225.
915 Neres, M., Terrinha, P., Custódio, S., Silva, S.M., Luis, J., Miranda, J.M., 2018. Geophysical evidence
916 for a magmatic intrusion in the ocean-continent transition of the SW Iberia margin.
917 Tectonophysics 744, 118-133.
918 Olivet, J.-L., 1996. Kinematics of the Iberian plate. Bulletin des Centres de Recherches Exploration-
919 Production Elf Aquitaine 20(1), 131-195.
920 Oudet, J., Münch, P., Borgomano, J., Quillevere, F., Melinte-Dobrinescu, M.C., Demory, F., Cornee,
921 J.-J., 2010. Land and sea study of the northeastern golfe du Lion rifted margin: the Oligocene–
922 Miocene of southern Provence (Nerthe area, SE France). Bull. Soc. Géol. Fr. 181(6), 591-607.
923 Pascal, G.P., Mauffret, A., Patriat, P., 1993. The ocean-continent boundary in the Gulf of Lion from
924 analysis of expanding spread profiles and gravity modelling. Geophys. J. Int. 113, 701-726.
925 Pedersen, T., Skogseid, J., 1989. Vøring Plateau volcanic margin: Extension, melting and rifting, Proc.
926 Ocean Drill. Program Sci. Results, 104, p00-01.
927 Réhault, J.-P., Boillot, G., Mauffret, A., 1984. The Western Mediterranean basin geological evolution.
928 Mar. Geol. 55, 447-477.
929 Réhault, J.-P., Honthaas, C., Guennoc, P., Bellon, H., Ruffet, G., Cotten, J., Maury, R.C., 2012.
930 Offshore Oligo-Miocene volcanic fields within the Corsica-Liguria Basin: Magmatic diversity
931 and slab evolution in the western Mediterranean Sea. J. Geodynamics 58, 73-95.
932 Reid, I.D., 1989. Effects of lithospheric flow on the formation and evolution of a transform margin.
933 Earth Planet. Sci. Lett. 95, 38-52.
934 Rollet, N., Déverchère, J., Beslier, M.O., Guennoc, P., Réhault, J.-P., Sosson, M., Truffert, C., 2002.
935 Back-arc extension, tectonic inheritance, and volcanism in the Ligurian Sea, western
936 Mediterranean. Tectonics 21 (3), 218-243.

Sauter, D., Unternehr, P., Manatschal, G., Tugend, J., Cannat, M., Le Quellec, P., Granath, J.W., 2016. Evidence for magma entrapment below oceanic crust from deep seismic reflections in the Western Somali Basin. Geology 44(6), 407-410.

Schärer, U., Kornprobst, J., Beslier, M.O., Boillot, G., Girardeau, J., 1995. Gabbro and related rock emplacement beneath rifting continental crust: UPb geochronological and geochemical constraints for the Galicia passive margin (Spain). Earth Planet. Sci. Lett. 130(1-4), 187-200.

Schettino, A., Turco, E., 2006. Plate kinematics of the Western Mediterranean region during the Oligocene and Early Miocene. Geophysical Journal International, 166(3), 1398-1423.

Séranne, M., 1999. The Gulf of Lion continental margin (NW Mediterranean) revisited by IBS: an overview. In: "The Mediterranean Basins: Tertiary Extension within the Alpine Orogen ", Durand, B., Jolivet, L., Horvatn, E., Séranne, M. (eds). Geological Society, London, Special Publications, vol. 156, p. 15-36.

Séranne, M., Benedicto, A., Labaume, P., Truffert, C., Pascal, G., 1995. Structural style and evolution of the Gulf of Lion Oligo-Miocene rifting: role of the Pyrenean orogeny. Mar. Petrol. Geol. 12(8), 809-820.

Shive, P.N., Frost, B.R., Peretti, A., 1988. The magnetic properties of metaperidotitic rocks as a function of metamorphic grade: implications for crustal magnetic anomalies. J. Geophys. Res. 93(B10), 12187-12195.

Sibuet, J.C., Srivastava, S., Manatschal, G., 2007. Exhumed mantle-forming transitional crust in the Newfoundland-Iberia rift and associated magnetic anomalies. J. Geophys. Res. 112(B6), B06105 doi:10.1029/2005JB003856.

Tavani, S., Bertok, C., Granado, P., Piana, F., Salas, R., Vigna, B., Munoz, J.A., 2018. The Iberia-Eurasia plate boundary east of the Pyrenees. Earth-Science reviews 187, 314-337.

Teixell, A., Labaume, P., Lagabrielle, Y., 2016. The crustal evolution of the west-central Pyrenees revisited: Inferences from a new kinematic scenario. C. R. Geoscience 348(3-4), 257-267.

Telford, W.M., Geldart, L.P., Sheriff, R.E., Keys, D.A., 1984. Applied Geophysics. Cambridge University Press, 860 pp.

Thybo, H., Artemieva, I.M., 2013. Moho and magmatic underplating in continental lithosphere. Tectonophysics 609, 605-619.

Tugend, J., Manatschal, G., Kusznir, N. J., Masini, E., Mohn, G., Thinon, I., 2014. Formation and deformation of hyperextended rift systems: Insights from rift domain mapping in the Bay of Biscay-Pyrenees. Tectonics 33(7), 1239-1276.

Vågnes, E., 1997. Uplift at thermo-mechanically coupled ocean continent transforms: Modeled at the Senja Fracture Zone, southwestern Barents Sea. Geo-Mar. Lett. 17, 100-109.

Vergés, J., Fernàndez, M., Martínez, A., 2002. The Pyrenean orogen: pre-, syn-, and post-collisional evolution. Journal of the Virtual Explorer 8, 55-74.

973 Vielzeuf, D., Kornprobst, J., 1984. Crustal splitting and the emplacement of Pyrenean lherzolites and
974 granulites. Earth Planet. Sci. Lett. 67(1), 87-96.
975 Vissers, R.L., Van Hinsbergen, D.J., Wilkinson, C.M., Ganerød, M., 2016. Middle Jurassic shear
976 zones at Cap de Creus (eastern Pyrenees, Spain): a record of pre-drift extension of the
977 Piemonte–Ligurian Ocean? J. Geol. Soc., London 174(2), 289-300.
978 Wang, Y., Chevrot, S., Monteiller, V., Komatitsch, D., Mouthereau, F., Manatschal, G., Benahmed, S.,
979 2016. The deep roots of the western Pyrenees revealed by full waveform inversion of
980 teleseismic P waves. Geology 44(6), 475-478.
981 Wehr, H., Chevrot, S., Courrioux, G., Guillen, A., 2018. A three-dimensional model of the Pyrenees
982 and their foreland basins from geological and gravimetric data. Tectonophysics 734-735, 16-32.
983 Wernicke, B., 1985. Uniform-sense normal simple shear of the continental lithosphere. Can. J. Earth
984 Sci. 22, 22.108-22.125.
985 White, R.S., McKenzie, D., 1989. Magmatism at rift zones: The generation of volcanic continental
986 margins and flood basalts. J. Geophys. Res. 94(B6), 7685-7729.
987 White, R.S., Spence, G.D., Fowler, S.R., McKenzie, D.P., Westbrook, G.K., Bowen, A.N., 1987.
988 Magmatism at rifted continental margins. Nature 330(6147), 439.
989 Ziegler, P.A., 1992. European Cenozoic rift system. Tectonophysics 208(1-3), 91-111.

990 **Figure captions**

991 **Fig. 1.** Magnetic anomaly map of the northwestern Mediterranean Sea showing the location of the
992 Gulf of Lion (GoL) (after Galdeano & Rossignol, 1977 and Schettino & Turco, 2006). Note the major
993 magnetic anomaly in the SW part of the GoL. Grey lines mark the boundaries of the continental,
994 transitional and oceanic domains from Gailler *et al.* (2009). The rectangle outlines the study area (see
995 **Fig. 3**).

996 **Fig. 2.** Structural setting of the GoL margin and surrounding area. Black lines represent the ECORS,
997 SARDINIA and LRM10 seismic profiles (see **Fig. 3**), the PYROPE E-W profile (Diaz *et al.*, 2018),
998 and sections M1 and M2 of this study (see **Fig. 7**). The location of the CMA is shaded in light pink.
999 Heavy grey dashed lines are boundaries between crustal domains I, II and III from Gailler *et al.*
1000 (2009). Transfer zones are only approximately located; the transfer zone labeled "1" is a hypothesized
1001 en echelon fault related to the Catalan transfer zone from Mauffret *et al.* (2001). Dark grey
1002 areas represent volcanic edifices. Offshore petroleum wells: Am, Agde Maritime; Au, Autan; Ca,
1003 Calmar; Ci, Cincindele; GLP1/GPL2, Golfe du Lion Profond 1/2; Mi, Mistral; Ra, Rascasse; Si,
1004 Sirocco; Tr, Tramontane. Mesozoic basins: Ag, Bas Agly basin; Bc, Boucheville basin; Bs, Beausset
1005 syncline; FM, Figueres-Montgrís basin; SPF, St. Paul de Fenouillet. The inset map shows major
1006 regional geological domains and structures (modified from Gorini *et al.*, 1993 edited by Séranne,
1007 1999). Dotted areas represent the oceanic domain (Langhian–Serravalian), crosshatching the Alpine
1008 orogen (Pliocene–Recent), dark grey the west European rift (Rupelian), and light grey the Pyrenean
1009 orogen (Eocene). Green dashed line, limit between two domains of different shallow crustal structures.

1010 **Fig. 3.** Schematic sections from the (A) ECORS , (B) SARDINIA and (C) LRM10 interpreted seismic
1011 profiles across the GoL margin (modified from Moulin *et al.* (2015), Séranne (1999) and Mauffret *et*
1012 *al.* (2001), respectively). Only the boundaries of the different layers used for modelling are drawn. The
1013 continental margin is divided into the continental domain (hinge zone, domain I), the transitional
1014 domain (domain II) and the oceanic domain (domain III). The intersection with cross-section M2 is
1015 shown. Triangles indicate projected locations of petroleum wells. LC, lower continental crust; OC,
1016 oceanic crust; UC, upper continental crust, PQ, plio-quaternary; M, miocene; S, synrift deposit; PB,
1017 paleaozoic basement. CC: continental

1018 **Fig. 4.** Complete Bouguer anomaly map of the study area; the inset map shows the coverage of the
1019 data used. The Bouguer reduction density used is 2300 kg/m^3. Also shown are the SARDINIA and
1020 ECORS seismic profiles and profiles M1 and M2 of this study. Note the gravimetric signals of a
1021 granitic pluton (GS) sampled by the Sirocco well and the NE-SW Nîmes fault. The inset shows the
1022 coverage of the gravimetric dataset: BGF and CGG gravity seafloor datasets (green), BGI (grey),
1023 IFREMER-SISMER (blue) and Elf-Explo-1996 (purple).

Fig. 5. RTP magnetic anomaly map of the study area. The CMA is the large positive feature in the western part of the GoL margin coinciding with the M1 and SARDINIA profiles. The smaller anomaly to its east is anomaly B (located by the letter B).

Fig. 6. Schematic diagram of geometric modelling. (A) Observed (bold curve) and modelled (thin curve) magnetic signals. (B) Observed and modelled gravimetric signals. (C) Model consisting of five layers representing water, sedimentary cover, upper crust, lower crust and mantle with their associated densities (kg/m^3).

Fig. 7. Proposed geophysical models M1 and M2, based on hypothesis H5 (**Table 1**). Locations in **Figs. 2** and **6**. Densities (ρ) are in kg/m^3 and magnetic susceptibilities (k) in SI. Materials 1 through 10 are as follows: 1, water layer (ρ = 2300; k = 0); 2, sedimentary cover (ρ = 2350, 2400, 2600; k = 0); 3, upper continental crust (ρ = 2700, 2750; k = 0); 4, lower continental crust (ρ = 2950; k = 0); 5, mantle (ρ = 3360; k = 0); 6, oceanic crust (ρ = 2850; k = 0); 7, lower part of the Catalan body (ρ = 3100; k = 0.11); 8, middle part of the Catalan body; (ρ = 3000; k = 0.1); 9, upper part of the Catalan body (ρ = 2800; k = 0.06); 10, transitional domain (ρ = 3100; k = 0). Main crustal domains of the GoL margin are drawn. The crossings between M1, M2 and SARDINIA, ECORS and PYROPE seismic profiles are indicated. The zero points in sections M1 and M2 correspond to the coasts of France and Spain, respectively.

Fig. 8. (A) Map showing Moho depth in the study area, compiled from the geophysical models of this study and previously published data. Dashed isobaths are from 3D geological modelling of Wehr *et al.* (2018); dot-dashed isobaths are compiled from Mauffret *et al.* (1995), Gallart *et al.* (2001), Nercessian *et al.* (2001), Mauffret *et al.* (2001), Gailler *et al.* (2009), Diaz *et al.* (2018), and others; solid isobaths are from this study. Question marks on where the connection between datasat was not straight forward. Grey areas represent the extent and thickness of the magnetic body of mafic rocks that generates the CMA. Hatched lines represent the transfer zones shown in **Figs. 1** and **2**. Note the northward mantle indentation between the M1 section and the ECORS profile. The lateral extension of the CTZ is represented by a red bracket. RB: Roussillon basin and CB: Catalan basin (B) ECORS and SARDINIA profiles and section M1 aligned on their crossing with section M2. Blue crosses and lines represent the location where the Moho rises to 15 km depth. See figure 2 for the precise location of the Catalan and Cathare basins and the Rascasse horst.

Table 1. Parameter values used for modelling, according to realistic geological assumptions. Petrophysical values are inspired by Telford *et al.* (1984), Guennoc *et al.* (1994), Berndt *et al.* (2001), Kearey *et al.* (2002), Keen *et al.* (2018) and Neres *et al.* (2018). Gradients are modelled by the use of multiple layers.

Figures

Figure 1

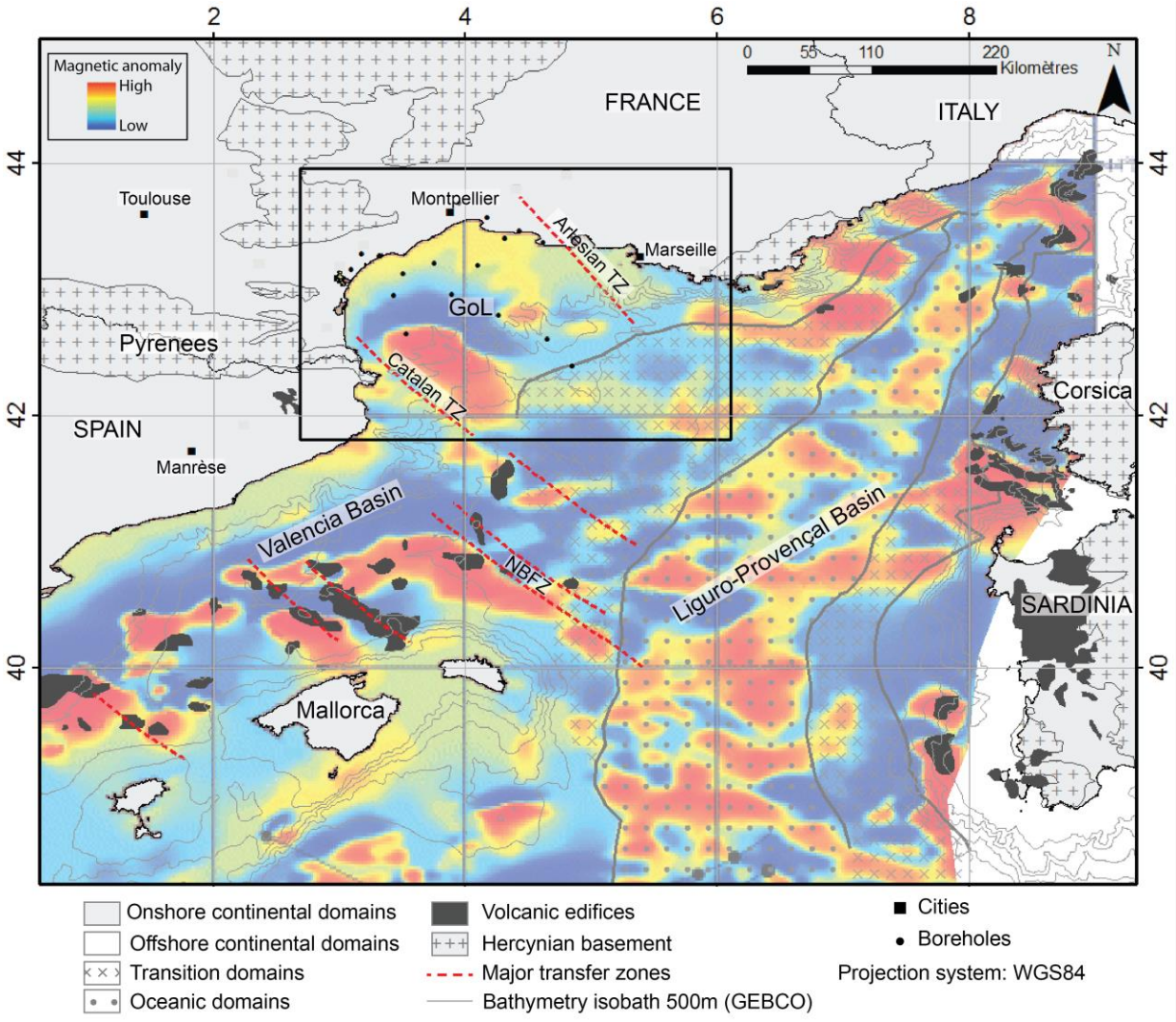


Figure 2

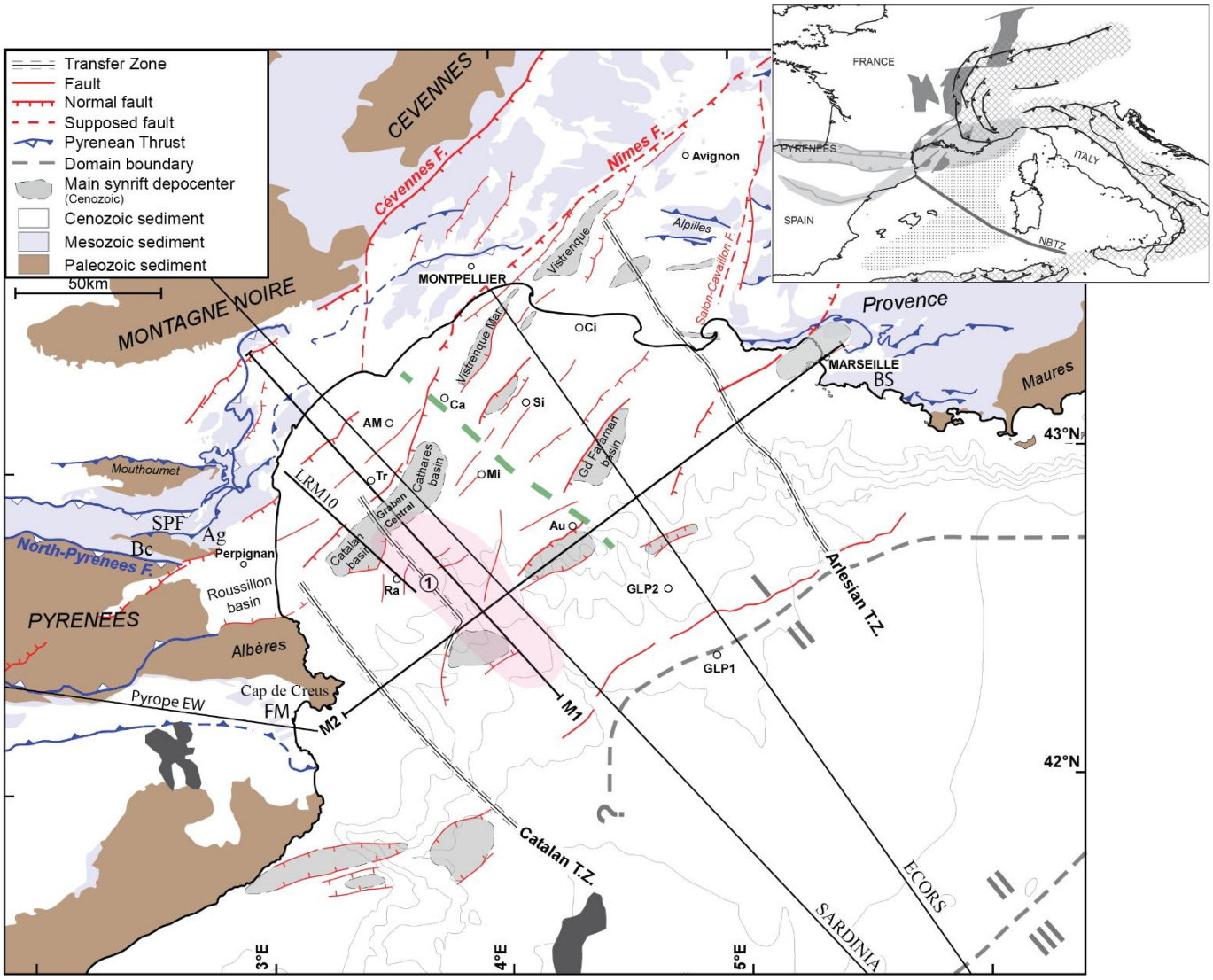

Transfer Zone
Fault
Normal fault
Supposed fault
Pyrenean Thrust
Domain boundary
Main synrift depocenter (Cenozoic)
Cenozoic sediment
Mesozoic sediment
Paleozoic sediment
50km
CEVENNES
Cévennes F.
Nîmes F.
Avignon
MONTAGNE NOIRE
MONTPELLIER
Vistrenque
Alpilles
Salon-Cavaillon F.
Provence
Vistrenque Marc
Ci
MARSEILLE
BS
Maures
43°N
Ca
Si
AM
Tr
Mi
Cathares basin
Gd Fa Aman basin
Mouthoumet
LRM10
Graben Central
Catalan basin
Au
SPF
Ag
Bc
Perpignan
North-Pyrenees F.
Roussillon basin
PYRENEES
Albères
Ra
GLP2
Arlesian T.Z.
GLP1
Pyrope EW
Cap de Creus
FM
M2
M1
42°N
Catalan T.Z.
SARDINIA
ECORS
3°E
4°E
5°E
FRANCE
PYRENEES
SPAIN
ITALY
NBTZ

Figure 3

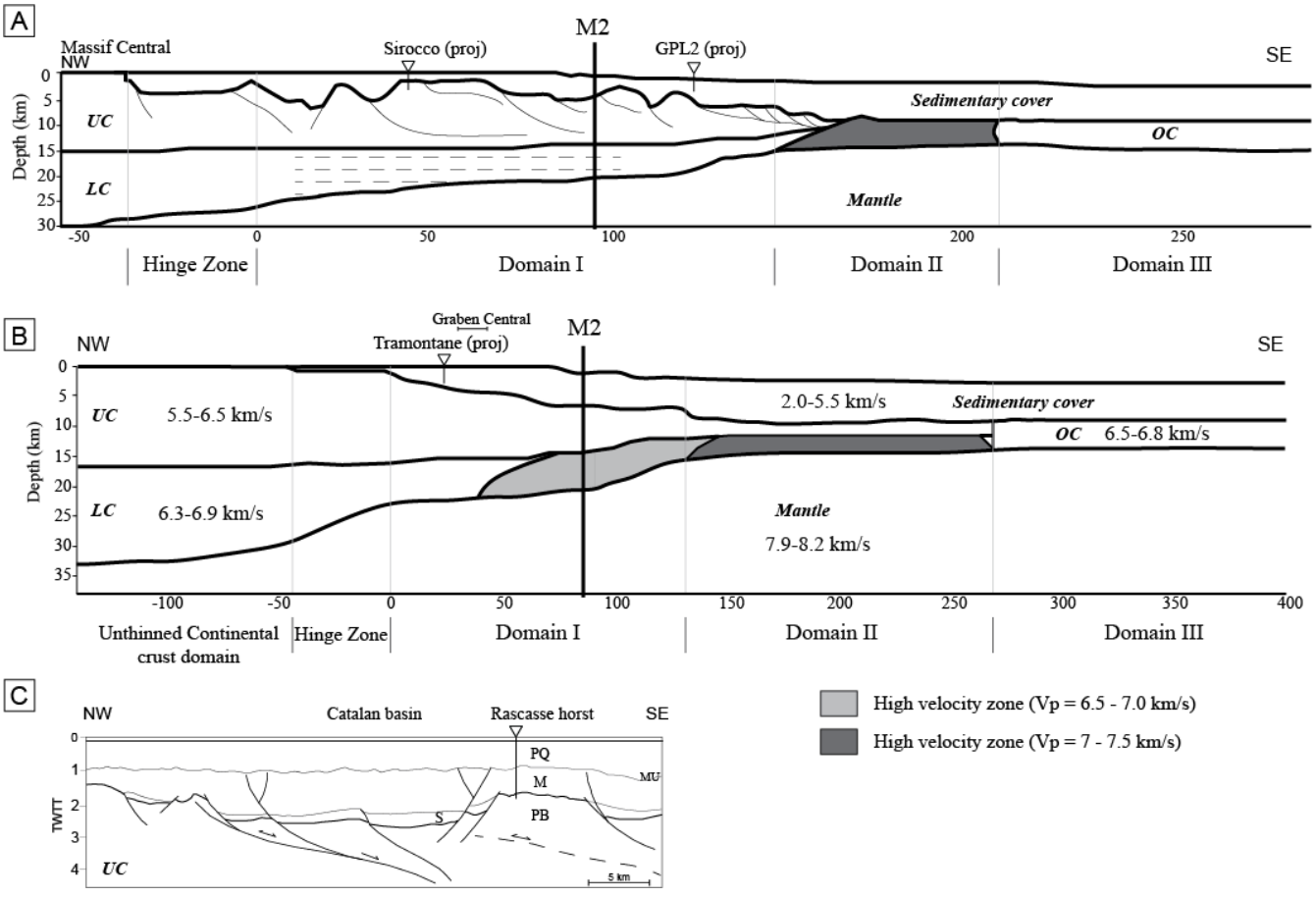

A
Massif Central
NW
Sirocco (proj)
M2
GPL2 (proj)
SE
Depth (km)
UC
LC
Sedimentary cover
OC
Mantle
Hinge Zone
Domain I
Domain II
Domain III
B
NW
Graben Central
Tramontane (proj)
M2
SE
UC
5.5-6.5 km/s
2.0-5.5 km/s
Sedimentary cover
OC
6.5-6.8 km/s
LC
6.3-6.9 km/s
Mantle
7.9-8.2 km/s
Unthinned Continental crust domain
Hinge Zone
Domain I
Domain II
Domain III
C
NW
Catalan basin
Rascasse horst
SE
TWTT
PQ
M
MU
S
PB
UC
5 km
High velocity zone (Vp = 6.5 - 7.0 km/s)
High velocity zone (Vp = 7 - 7.5 km/s)

Figure 4:

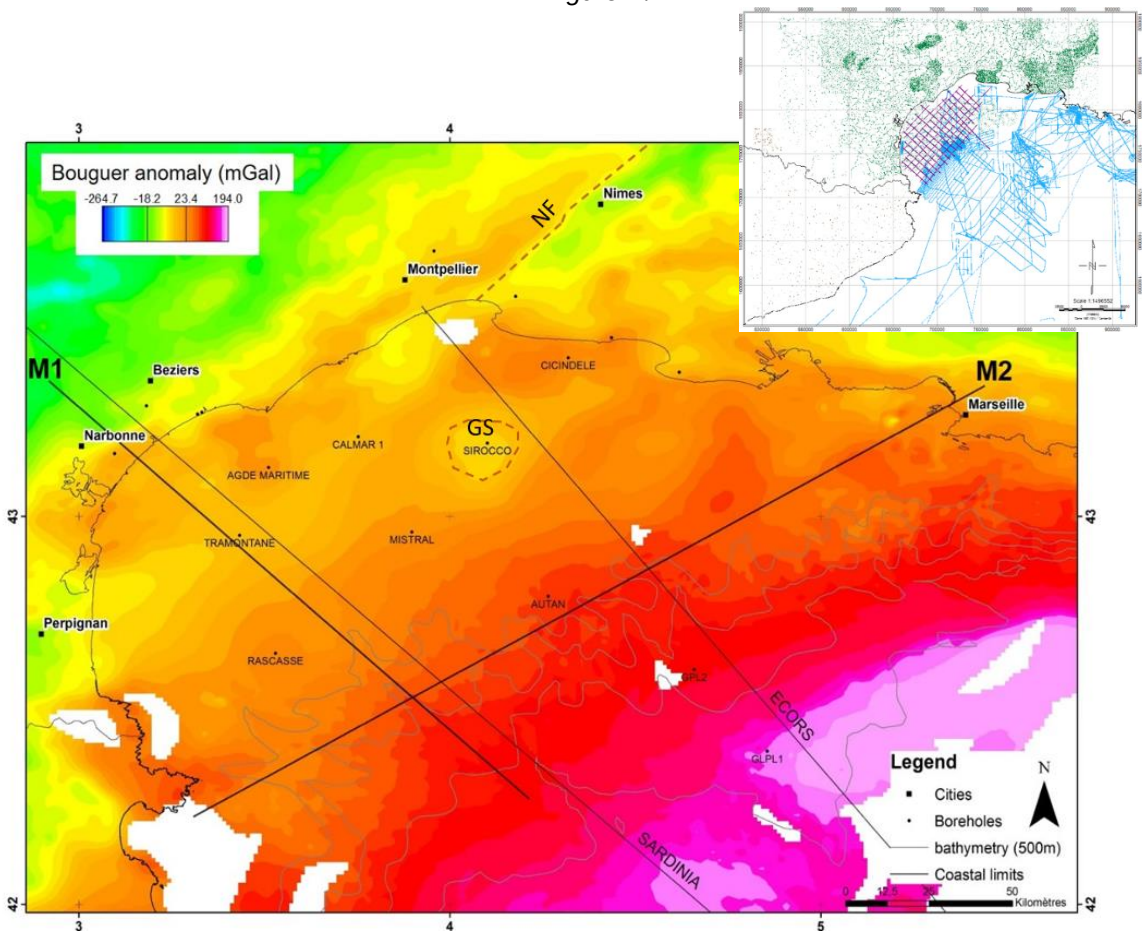

Bouguer anomaly (mGal)
-264.7 -18.2 23.4 194.0
NF
Nimes
Montpellier
M1
Beziers
CICINDELE
M2
Marseille
Narbonne
GS
SIROCCO
CALMAR 1
AGDE MARITIME
TRAMONTANE
MISTRAL
AUTAN
Perpignan
RASCASSE
ECORS
SARDINIA
Legend
Cities
Boreholes
bathymetry (500m)
Coastal limits
N
Kilomètres
3
4
5
42
43

Figure 5

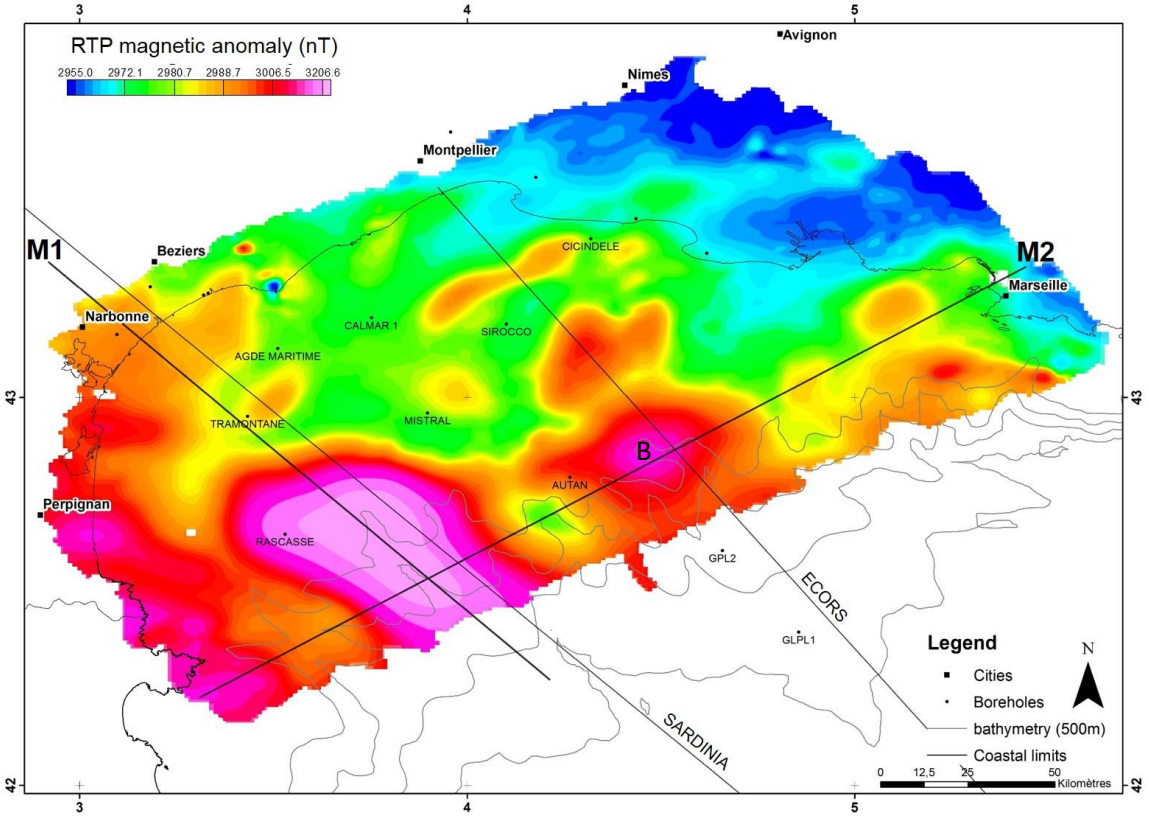

RTP magnetic anomaly (nT)
2955.0 2972.1 2980.7 2988.7 3006.5 3206.6
Avignon
Nimes
Montpellier
Beziers
Narbonne
Perpignan
Marseille
M1
M2
B
CICINDELE
CALMAR 1
SIROCCO
AGDE MARITIME
TRAMONTANE
MISTRAL
AUTAN
RASCASSE
GPL2
GLPL1
ECORS
SARDINIA
Legend
Cities
Boreholes
bathymetry (500m)
Coastal limits
N
0 12,5 25 50 Kilomètres
3
4
5
43
42

Figure 6

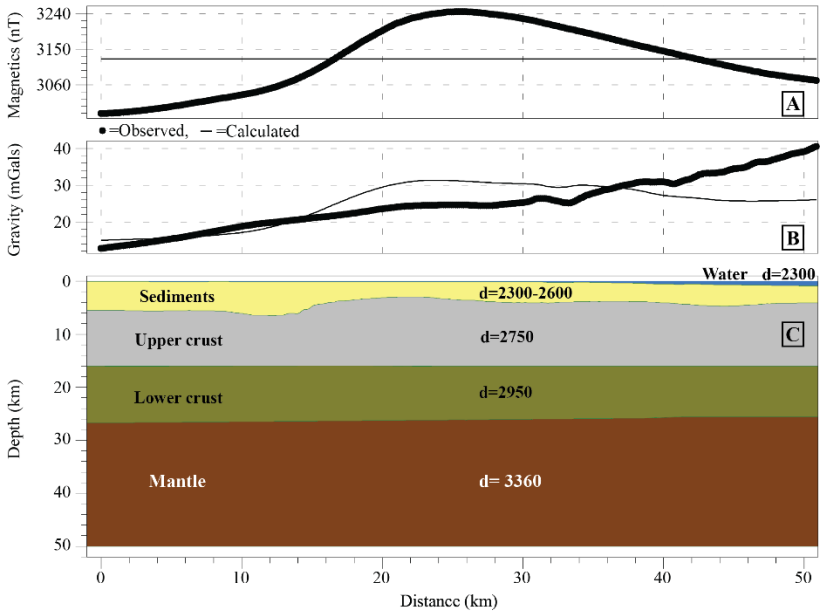


Table 1.–

Hypotheses		Density (Kg/m^3)	Magnetic Susceptibility (SI)	Maximum thickness (km)	Adjusted with the data	
					Magnetic	Gravimetric
H1	Basalt at the top of the upper crust	2850	0.18	4	~	x
H2	Basalt (1) at the top of the upper crust and gabbro (2) into the lower crust	(1) 2850 (2) 3000	0.15 0.10	4.5 5	~	x
H3	Basalt at the limit between the two crust	2850	0.1	8	√	x
H4	Gabbro between the upper crust and the mantle	3000	0.1	10	√	x
H5	Gabbro between the upper crust and the mantle with a petrophysical gradient (from top to bottom)	2800 3000 3100	0.06 0.1 0.11	2 7 2	√	√
H6	Serpentinized mantle	2700	0.1	10	√	x
H7	Serpentinized mantle, with a petrophysical gradient (from top to bottom)	2700 2850 2900 3000	0.3 0.15 0.09 0.005	>1 2 5 2.2	√	x

Figure 7

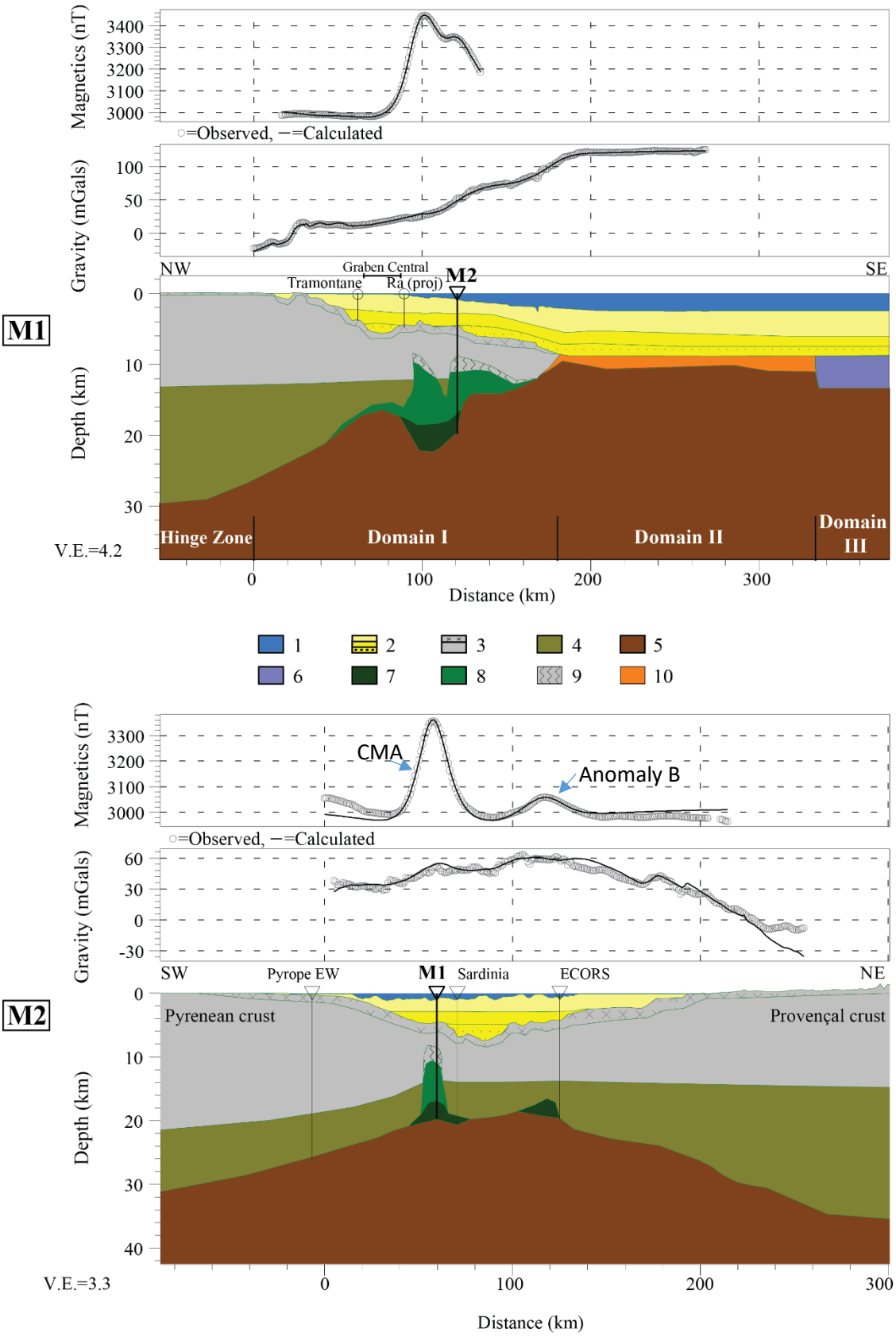
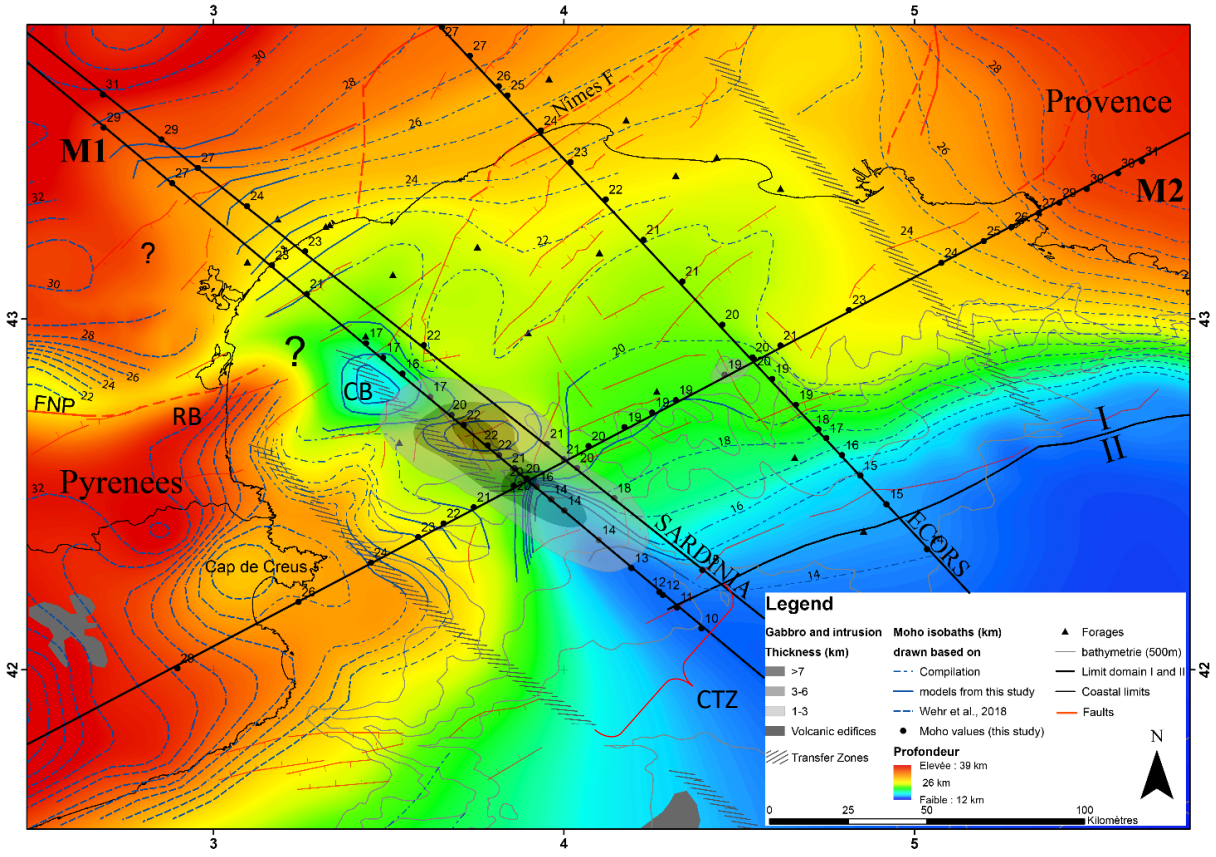
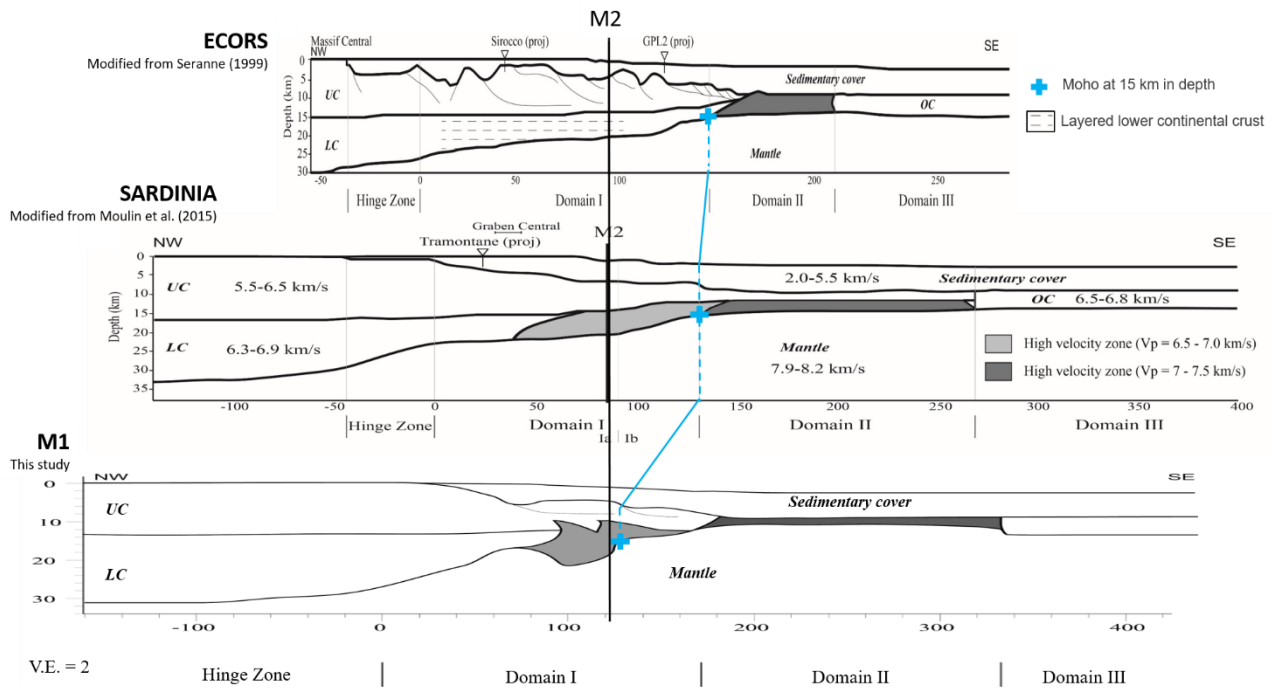

M1
Magnetics (nT)
3400
3300
3200
3100
3000
○=Observed, —=Calculated
Gravity (mGals)
100
50
0
NW
SE
Graben Central
Tramontane
Ra (proj)
M2
Depth (km)
0
10
20
30
Hinge Zone
Domain I
Domain II
Domain III
V.E.=4.2
0
100
200
300
Distance (km)
1
2
3
4
5
6
7
8
9
10
M2
Magnetics (nT)
3300
3200
3100
3000
CMA
Anomaly B
○=Observed, —=Calculated
Gravity (mGals)
60
30
0
-30
SW
Pyrope EW
M1
Sardinia
ECORS
NE
Depth (km)
0
10
20
30
40
Pyrenean crust
Provençal crust
V.E.=3.3
0
100
200
300
Distance (km)

Figure 8

a)


M1
M2
Provence
Nimes F.
Pyrenees
FNP
RB
CB
Cap de Creus
SARDINIA
ECORS
CTZ
I
II
Legend
Gabbro and intrusion Thickness (km)
>7
3-6
1-3
Volcanic edifices
Transfer Zones
Moho isobaths (km) drawn based on
Compilation
models from this study
Wehr et al., 2018
Moho values (this study)
Profondeur
Elevée : 39 km
26 km
Faible : 12 km
Forages
bathymetrie (500m)
Limit domain I and II
Coastal limits
Faults
N
0 25 50 100 Kilomètres

b)


ECORS
Modified from Seranne (1999)
M2
Massif Central
Sirocco (proj)
GPL2 (proj)
NW
SE
Depth (km)
UC
LC
Sedimentary cover
OC
Mantle
Moho at 15 km in depth
Layered lower continental crust
Hinge Zone
Domain I
Domain II
Domain III
SARDINIA
Modified from Moulin et al. (2015)
Graben Central Tramontane (proj)
5.5-6.5 km/s
6.3-6.9 km/s
2.0-5.5 km/s
6.5-6.8 km/s
7.9-8.2 km/s
High velocity zone (Vp = 6.5 - 7.0 km/s)
High velocity zone (Vp = 7 - 7.5 km/s)
Ia
Ib
M1
This study
V.E. = 2